Jason K. Karimy

Jkkarimy@gmail.com

EDUCATION

University of Maryland Baltimore
Baltimore, Maryland 08/14 – 05/16
M.S. in Molecular Medicine

University of Colorado at Denver
Denver, Colorado 01/09 – 05/12
Cum laude B.S. in Biological Science with a minor in Mathematical Science and Psychology

University of Northern Colorado
Greeley, Colorado 08/05 – 12/07

RESEARCH EXPERIENCE

University of Maryland, Baltimore, Baltimore, MD
Research Assistant in the lab of J. Marc Simard, MD, PhD. 06/12 – 05/16
Research Projects: Molecular mechanisms behind the formation of hydrocephalus following intraventricular hemorrhage.

Oregon Health and Science University, Portland, OR
Summer Research Student in the lab of Mary Stenzel-Poore, PhD. 05/11 – 08/11
Research Projects: Overexpression of IFIT-1 gene in murine primary cortical cells via Lentivirius.

Oregon Health and Science University, Portland, OR
Summer Research Student in the lab of Mary Stenzel-Poore, PhD. 05/10 – 08/10
Research Projects: Investigation of the mechanisms behind neuroprotection: TNF-a induction in IRF3/7 and IFNR knockout mice.

University of Colorado at Denver
Student Researcher in the lab of Michele Engel, PhD. 01/10 – 05/10
Research Projects: Molecular techniques for isolating differentially expressed genes in polycyclic aromatic hydrocarbons.

Swedish Medical Center, Denver, CO
Student Researcher in the lab of G. Alexander West MD, PhD 08/09 – 08/10
Research Projects: Electrophysiology in hippocampal organotypic cultures.
Effects of cocaine on endothelial vessels in the brain.

Swedish Medical Center, Denver, CO
Summer Research Intern in the lab of G. Alexander West MD, PhD 05/09 – 08/09
Research Projects: Oxygen glucose deprivation of organotypic and dissociated cell cultures for the study of mechanisms behind stroke.

PUBLICATIONS

Complications associated with decompressive craniectomy; A systematic review.
Authors: Kurland, DB, Khaladj-Ghom A, Stokum JA, Carusillo B, **Karimy JK**, Gerzanich V, Sahuquillo J, Simard JM.
Neurocritical Care: June 2015; DOI 10.1007/s12028-015-0144-7

A novel method to study cerebrospinal fluid dynamics in rats.
Authors: **Karimy JK**, Kahle KT, Kurland DB, Yu E, Gerzanich V, Simard JM.
J Neurosci Methods: Jan 2015; 241 (2015) 78-84.

Glibenclamide for the Treatment of Acute CNS Injury.
Authors: Kurland DB, Tosun C, Pampori A, **Karimy JK**, Caffes NM, Gerzanich V, Simard JM.
Pharmaceuticals: Oct 2013; 6(10): 1287–1303.

AWARDS & COMMENDATIONS

Undergraduate Research Opportunity Program Award Winner 2010-2011
Molecular Genetics: *Gene expression changes in Trametes Versicolor during polycyclic aromatic hydrocarbon degradation.*

POSTERS & ORAL PRESENTATIONS

Society for Neuroscience at Chicago, Illinois 10/15
Poster Presentation*: An application of a novel method to study cerebrospinal fluid dynamics in rats.*
Authors: **Jason K. Karimy**, K.T. Kahle, D.B. Kurland, V. Gerzanich, J.M. Simard.

2014 AANS/CNS Section on Pediatric Neurological Surgery Annual Meeting at Amelia Island, Florida 12/14
Poster Presentation*: Pharmacotherapeutic Targeting of a Novel Inflammation-Induced Switch of CSF Dynamics in Intraventricular Hemorrhage-Associated Hydrocephalus.*
Authors: Kristopher T. Kahle, **Jason Karimy**, Volodymyr Gerzanich and J. Marc Simard

Neuroscience 2014 at Washington, DC 11/14
Poster Presentation*: Primary adult rat microglia express Sur-1 regulated channels.*
Authors: D.B. Kurland, N. Caffes, **J.K. Karimy**, V. Gerzanich, J.M. Simard.

18th Annual VAMHC Research Day at Baltimore, Maryland 5/14
Poster Presentation*: Glibenclamide treatment as a prophylaxis against blast-TBI in rat blast model.* Authors: K. Keledjian, A. Pampori, **J. Karimy**, C. Tosun, V. Gerzanich, J.M. Simard.

Regional Society for Neuroscience at Baltimore, Maryland 11/13
Poster Presentation*: Bumetanide Reduces CSF Production – A Novel Therapeutic Option for Intraventricular Hemorrhage.*
Authors: **Jason K. Karimy**, David B. Kurland, V. Gerzanich, J.M. Simard.

Research and Creative Activities Symposium at UC Denver 04/10
Poster Presentation*: Immunocytochemistry in organotypic and dissociated cell cultures for investigation of therapeutics in stroke.* This project focused on finding optimal conditions for detecting neuronal and glial cell death in murine hippocampal organotypic cultures under oxygen-glucose deprivation.

Research Presentation in the lab of Mary Stenzel-Poore, PhD. 08/11
Oral Presentation: summarized summer research: *Overexpression of IFIT-1 gene in murine primary cortical cells via Lentivirius.*

Research Presentation in the lab of Mary Stenzel-Poore, PhD. 08/10
Oral Presentation: summarized summer research: *Investigation of the mechanisms behind neuroprotection: TNF-□ induction in IRF3,7 and IFNR knockout mice.*

VOLUNTEERING & CLINICAL SHAWDOWING

Clinical Shadowing of G. Alexander West MD, PhD 03/09 – 05/12

- Attending rounds, observing doctor-patient interaction, trained to read MRI's.
- Observed various types of neurosurgery

Over 1000 hours Swedish Medical Center volunteer

- Worked as an assistant in the post-anesthesia care unit (PACU) creating charts.
- Worked at the front desk of the hospital answering phones and directing patients to their destination.

Teaching Experience

Honors Chemistry and Honors Calculus Tutor at University of Colorado Denver
Held office hours and group tutoring sessions 8/11 – 5/12

Immunology Teacher Assistant at University of Colorado Denver
Attended class, held office hours, proctored and graded exams 8/11 - 5/12

Biology II Teacher Assistant and Grader at University of Colorado Denver
Attended class, provided tutoring, proctored and graded exams 1/10 – 5/10

Abstract

Intraventricular hemorrhage (IVH), is the accumulation of blood within the ventricles, and is associated with high morbidity and mortality via IVH-associated hydrocephalus (IVHH). IVHH distorts the surrounding brain tissue, resulting in cognitive and motor impairments, or death. IVHH is attributed to impaired CSF reabsorption at the arachnoid granulations; however, the contribution of CSF hypersecretion is unknown. NKCC1 is regulated by SPAK via phosphorylation, and is critical to the formation of CSF. A novel method to measure the rate of CSF secretion was used to study the role of the SPAK-NKCC1 pathway in IVHH. IVH resulted in ventriculomegaly, due to a 3-fold increase in CSF secretion, determined to be due to SPAK-mediated phosphorylation of NKCC1. Methods to inhibit phosphorylation of NKCC1 significantly attenuated the hypersecretion of CSF and ventriculomegaly associated with IVHH. These results provide evidence that the SPAK-NKCC1 pathway drives the pathogenesis of IVHH and is a potential therapeutic target.

Molecular Mechanisms of CSF Hypersecretion in Intraventricular Hemorrhage-associated Hydrocephalus

Jason K. Karimy

Thesis submitted to the Faculty of the Graduate School of the
University of Maryland, Baltimore in partial fulfillment
of the requirements for the degree of
Master of Science
2016

Dedication

I want to dedicate my thesis to my parents and Dr. G. Alexander West. Without the support of these people I would not have made it this far.

Acknowledgements

I would like to start by thanking my thesis committee. Dr. Frank Margolis, Dr. Brian Mathur, Dr. Volodymyr Gerzanich and Dr. J. Marc Simard.

First, I would like to thank Dr. Gerzanich. He has tirelessly mentored me over the past four years. He has spent days, nights and weekends teaching me. He is irreplaceable and truly a phenomenal scientist and teacher.

Additionally, I would like to thank Dr. Kristopher T. Kahle, who has collaborated on this project from its beginning. I want to thank him for his mentorship, continued interest in this project, and the opportunity to continue working with him as I head to Connecticut for medical school.

I would also like to thank all the people in the Simard lab. One of the reasons the Simard lab will always be my home is because the quality of people within it.

My fellow graduate students and closest friends Jesse A. Stokum, Brianna Carusillo and David B. Kurland. I have had the pleasure of working with three of the most intelligent, wonderful, kind, interesting, weird…etc. people over the past four years. These people are my family, and although I am very excited for my future, and theirs, I am sad to see our time in the Simard lab coming to an end. Fortunately, there will always be the Hamptons!

Finally, I want to extend my deepest thanks to Dr. Simard. Under Dr. Simard's guidance I have grown as scientist and as a person. The four years I have spent learning from him have been the most formative years of my life. He represents excellence and forever has my gratitude and admiration.

Table of Contents

Table of Figures

CHAPTER 1

INTRODUCTION

Stroke and intraventricular hemorrhage

Stroke is a devastating disease that affects 795,000 people, killing 130,000 and placing an annual $33 billion burden on the US economy.[1, 2] Hemorrhagic stroke has the highest degree of morbidity and mortality among any subgroup of stroke, and accounts for 15% of the total number of stroke cases.[1, 3, 4] Intraventricular hemorrhage (IVH), a subtype of hemorrhagic stroke, is the accumulation of blood within the ventricles. IVH can occur spontaneously or, more commonly, as a secondary injury resulting from intracerebral or subarachnoid hemorrhage. The presence of IVH confers poor prognosis, significantly exacerbating the clinical outcomes of diseases, and is associated with 50%-80% mortality when co-occurring as a secondary injury.[4-7]

Complications and treatments of IVH

A major complication of IVH is hydrocephalus, a pathological accumulation of cerebrospinal fluid (CSF) in the ventricular system. Hydrocephalus can result in ventriculomegaly (enlargement of the ventricles), which may cause severe neurological dysfunction or death[6]. IVH-associated hydrocephalus (IVHH) can deform brain tissue via elevated intracranial pressure (ICP) and can cause mechanical damage to periventricular white matter, ultimately resulting in a cascade of insults that include ischemia, inflammation, and free radical injury. The standard treatments for IVHH are CSF diversion methods via a subcutaneous shunt catheter from the ventricular space to another part of the body, where the CSF can be reabsorbed (ventriculoperitoneal, ventriculopleural shunt), or an external ventricular drain (EVD) where the CSF collects in a vessel outside the body. These procedures often fail, require revision, and seed infections, all of which can cause additional complications.[8-12] Overall, current IVHH treatments are invasive and often lead to sub-optimal outcomes. Therefore, minimally invasive therapeutics to treat IVHH must continue to be explored.

Pathogenesis of IVHH

The molecular pathophysiology of IVHH remains poorly understood.[13] Historically, IVHH has been attributed to impaired CSF reabsorption at the arachnoid granulations by a congealed blood clot, and/or inflammation resulting in fibrosing arachnoiditis, meningeal fibrosis, and subependymal gliosis.[6, 12-14] However, evidence supporting reduced reabsorption of CSF is sparse, suggesting that other mechanisms could be involved.[15]

Alternatively, overproduction of CSF may be involved in the pathogenesis of IVHH. Indeed, other secretory epithelia, such as those in the intestine, lung, and pancreas respond to irritating or pro-inflammatory stimuli by hypersecretion of fluid (e.g. diarrhea,[16] asthma,[17] pancreatitis[18]). In addition, in pathological conditions such as villous hypertrophy or papilloma of the choroid plexus, an increase in CSF secretion is known to cause hydrocephalus.[19-24] Thus, it is possible that the choroid plexus epithelium (CPE) exhibits hypersecretion in response to inflammatory stimuli, such as blood.[25]

Mechanisms of CSF secretion

The CPE generates the majority of CSF, at a rate of ~0.4 mL per minute per gram of tissue - a secretion rate that is only rivaled by the renal proximal tubule and the pancreatic ducts.[26] CSF secretion is achieved through the net transport of solutes (Na^+, Cl^-, and HCO_3^-, along with the recycling of K^+) across the CPE into the ventricles via ion transporters and channels expressed on the CPE apical and basolateral membranes. Net solute influx results in a trans-epithelial osmotic gradient, which favors osmotically-driven transcellular and paracellular movement of water across the CPE and ependyma.

Many of the individual ion channels and transporters involved in ion and water transport required for CSF formation are known. Na^+-K^+-$2Cl^-$ isoform 1 (NKCC1) is an electroneutral ion cotransporter of one Na^+, one K^+, and two Cl^- across the plasma membrane.[26] In almost all secretory epithelia, NKCC1 mediates ion influx and is situated on the basolateral membrane. Interestingly, NKCC1 is expressed on the apical (luminal) membrane of the CPE and mediates both inward and outward-directed transport.[26-29] Thus, it is likely that NKCC1 is highly-regulated in the CPE.

Regulation of NKCC1 in secretory epithelium

Less well known are the upstream mechanisms that regulate these ion transport molecules to influence the rate of production and the composition of CSF.[26, 30, 31] In other secretory epithelium the Ste20/SPS1-related proline-alanine-rich protein kinase (SPAK) associates with NKCC1 via a CCT binding module in SPAK and a (R/K)FX(V/I) binding motif in NKCC1,[32] and stimulates NKCC1 via direct phosphorylation at Thr203/Thr207/Thr212.[33, 34] The importance of SPAK in the regulation of ion transport in renal,[35, 36] intestinal,[35, 37] and pancreatic[35, 38] epithelia is well documented. However, a potential role in the CPE for SPAK-NKCC1 mediated IVHH has not been well studied.

Goals of the present study

An important impediment to progress in this field is the lack of a suitable method for quantifying real-time CSF formation in laboratory rodents in vivo under near-physiological conditions. Oreskovic and Klarica recently reviewed the most common methods that have been used to measure CSF formation.[39] They identified important shortcomings with almost all of these methods, many of which provide indirect measures of CSF formation that require assumptions which may be difficult to justify.[39, 40] Other methods that provide direct measures of CSF formation require the use of non-physiological conditions or have been implemented only in larger animals such as sheep and cats. Therefore, the first aim of this thesis was to develop a reproducible method that permits the real-time measurement of the rate of formation of CSF in laboratory rats, in vivo, under near-physiological conditions. The second aim of this thesis was to determine if hypersecretion of CSF plays a role in the formation of IVHH, and if so, whether intraventricular modulation of the SPAK-NKCC1 pathway in the CPE could impact the development of hydrocephalus.

CHAPTER 2

DEVELOPMENT OF A NOVEL MODEL TO STUDY CSF DYNAMICS

Materials and Methods

Animals

Animal experiments were performed under a protocol approved by the Institutional Animal Care and Use Committee (IACUC) of the University of Maryland, and in accordance with the guidelines and regulations in the NIH Guide for the Care and Use of Laboratory Animals. Male Wistar rats, ages 8–12 weeks (Harlan, Indianapolis, IN, USA), were anesthetized (60 mg/kg ketamine plus 7.5 mg/kg xylazine, IP) and allowed to breathe room air spontaneously. Body temperature was maintained at $37 \pm 1^{\circ}$C (Harvard Apparatus, Holliston, MA, USA) throughout the course of the experiments.

Procedure for measuring CSF formation

Anesthetized rats were mounted in a stereotactic apparatus (Stoelting Co., Wood Dale, IL) in the usual manner with an incisor-bar and ear-bars (Fig. 1). A midline scalp incision was made to expose the skull. A 1.3-mm burr hole, centered over the left lateral ventricle (x, −0.8 mm; y, +1.7 mm relative to bregma), was made using a high-speed drill. The dura and underlying arachnoid and pia were opened using a cruciate incision made with the tip of a #11 scalpel blade. The wound was irrigated with sterile normal saline (NS) to clear any blood. After completing the burr hole and opening the membranes, the hind end of the animal was elevated ∼2 cm, the incisor-bar was removed, the rat's head was rotated on the ear-bars 90°, nose-down, and was held in this vertical position using an improvised plastic device pressing against the dorsum of the snout. The cisterna magna was exposed by dissecting the suboccipital muscles from the occipital bones and exposing the atlanto-occipital ligament. The ligament was partially resected and the underlying dura was punctured in the midline to enter the cisterna magna, with the size of the dural puncture being ∼1 mm^2. A 23 gauge flexible catheter (PE-20) loaded with sterile, molecular grade mineral oil (Sigma Aldrich, St. Louis, MO) pre-warmed to 37°C was advanced gently 5 mm through the foramen of Magendie into the 4th ventricle. Mineral oil (100 µL) was infused into the 4th ventricle to occlude the aqueduct of Sylvius. Following occlusion of the aqueduct, with the long axis of the head still positioned vertically, the left lateral ventricle was cannulated using a pre-marked glass capillary tube (cat # CV8010-300; borosilicate; OD, 1 mm; ID, 0.8 mm; length, 30 cm; VitroCom, Mountain Lakes, NJ). The capillary tube was held horizontally in the correct "x" and "y" planes (now rotated 90°), and was carefully advanced by hand horizontally through the burr hole to a "z" coordinate of 4 mm to enter the frontal horn of the lateral ventricle. The capillary tube, which often contained brain matter, was withdrawn and was replaced by a new capillary tube that was reintroduced into the ventricle. After entering the ventricle, the capillary tube began to fill with CSF, with the front of fluid advancing steadily in the capillary tube as CSF was formed. The distance that the front traveled within the capillary tube was measured at precise intervals (5 or 10 min). The volume of CSF that formed was calculated as: $V\ (mm^3) = \pi \cdot r^2 \cdot d$. The rate of CSF formation (µL/min) was calculated as the slope of the volume–time relationship. In a separate series of experiments, the effect of collecting CSF at elevated outflow pressures (1.5 and 3 cm of H_2O) was examined. For these experiments, the outflow capillary tube was modified by introducing two right-angle bends, 3 cm apart, to create a "Z" shape. Rotating the Z-shaped outflow capillary tube allowed measurements at different outflow pressures to be made in the same rat– when the plane of the “Z” was oriented horizontally, the outflow pressure was 0 cm of H_2O; when the plane of the “Z” was rotated 45° from horizontal, the outflow pressure was 1.5 cm of H_2O; when the plane of the “Z” was rotated 90°from horizontal, the outflow pressure was 3 cm of H_2O.

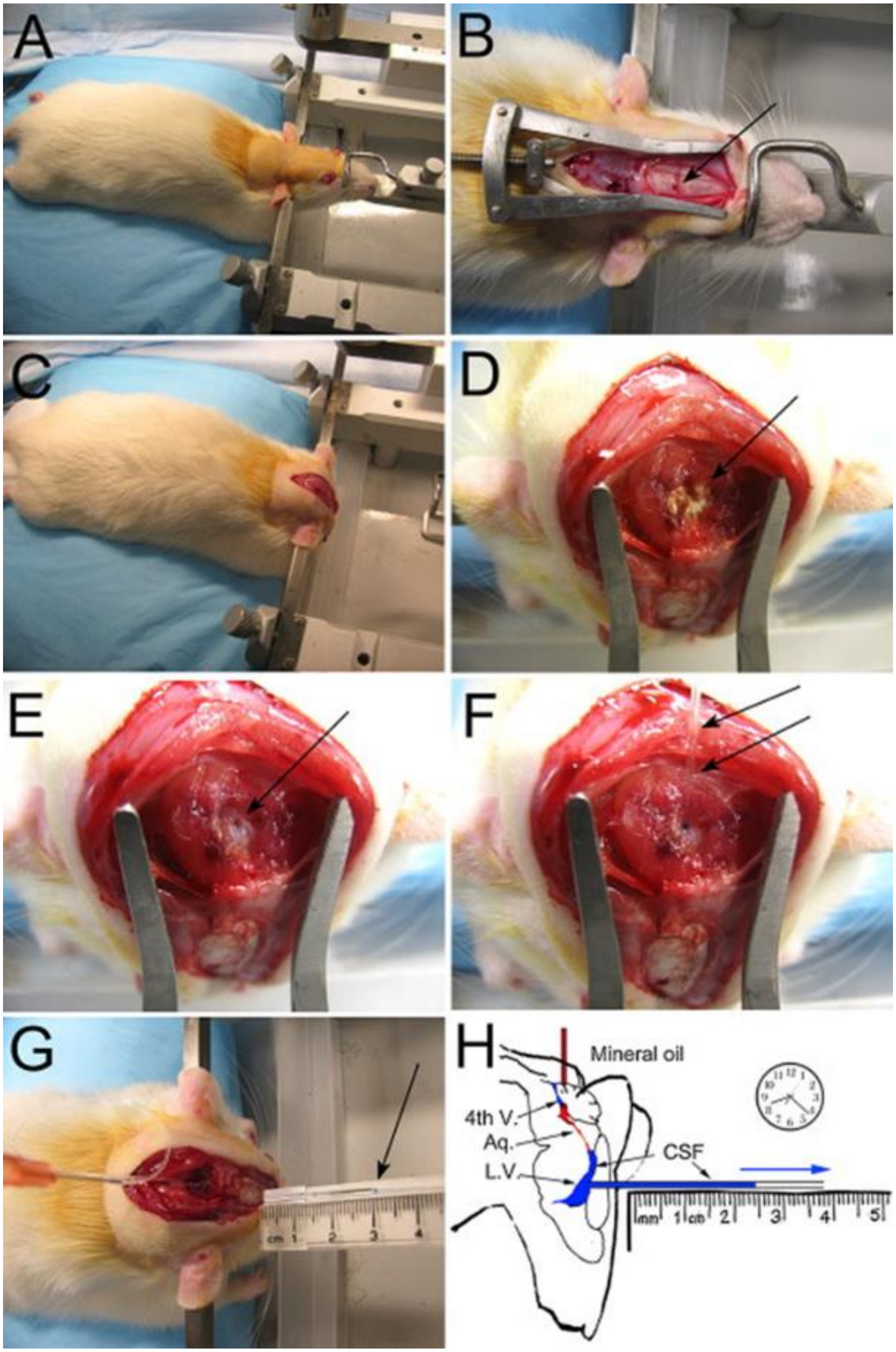
A
B
C
D
E
F
G
cm 1 2 3 4
H
Mineral oil
4th V.
Aq.
L.V.
CSF
mm 1 cm 2 3 4 5

Figure 1. The experimental procedure for measuring CSF formation.
Photographs (A–G) and artistic depiction (H) of the procedure for measuring CSF formation. An anesthetized rat is mounted in a stereotactic apparatus (**A**); a midline scalp incision is made to expose the skull, and a 1.3-mm burr hole, centered over the left lateral ventricle (x, −0.8 mm; y, +1.7 mm relative to bregma), is made (**B**, arrow); the hind end of the animal is elevated ∼2 cm, the incisor-bar is removed, the rat's head is rotated on the ear-bars 90°, nose-down, and is held in this vertical position (**C**); the suboccipital muscles are bluntly dissected to expose the atlanto-occiptal ligament (**D**, arrow); the ligament is partially resected and the underlying dura is punctured in the midline (**E**, arrow); a 23 gauge flexible catheter (PE-20) loaded with sterile, molecular grade mineral oil pre-warmed to 37°C is advanced gently 5 mm through the foramen of Magendie into the 4th ventricle for infusion of mineral oil (100 µL) into the 4th ventricle to occlude the aqueduct of Sylvius (**F**, arrows); the left lateral ventricle is cannulated using a pre-marked glass capillary tube held horizontally in the correct "x" and "y" planes (now rotated 90◦), and is carefully advanced by hand horizontally through the burr hole to a "z" coordinate of 4 mm to enter the frontal horn of the lateral ventricle, allowing CSF to exit (**G**, arrow); the distance traveled by the advancing front of fluid is used to calculate the rate of CSF formation (**H**).

Procedure for infusing drugs

In some rats, before rotating the head to a vertical orientation, a second burr hole was made over the right lateral ventricle (x: −0.8 mm, y: −1.7 mm relative to bregma) and the 28-gauge cannula from an Alzet brain infusion kit (#1; Durect, Cupertino, CA), with a single spacer to adjust the depth to 4.5 mm, was stereotactically placed in the ventricle and secured to the skull using cyanoacrylate adhesive. The cannula was connected via a PE-20 catheter to a 1 mL syringe containing an infusion solution (see below). The syringe was loaded into a syringe infusion apparatus (Pump elite 11, Harvard Apparatus) and maintained at 37◦C. Intraventricular infusions were performed at a nominal pump rate of 2 µL/min. The actual rate of fluid delivery by the pump was determined empirically in a separate experiment, performed in triplicate, in which the volume of fluid delivered was measured over the course of 30 min. The actual rate was 1.93 ± 0.03 µL/min. When measuring CSF formation during intraventricular drug infusion, the "actual infusion rate" of 1.93 µL/min was subtracted from the "measured outflow rate" to obtain the "calculated rate of CSF formation". When measuring the effect of a drug (acetazolamide or mannitol, see below), first the baseline rate of CSF formation was determined during spontaneous CSF formation (no infusion), then the calculated rate of formation was determined after switching to the test drug. The infusion then was stopped, to check for reversibility of the drug effect. Intraventricular infusion solutions were made using artificial CSF (aCSF), composed as follows (in mM): Na 150; K 3.0; Ca 1.4; Mg 0.8; P 1.0; Cl 155, pH 7.19 (Tocris, Bristol, UK), with a calculated osmolarity of 311.2 $mOsm_C$/L. Two drugs were studied, acetazolamide (45 mM; Sigma Aldrich, St. Louis, MO) and mannitol (88.2 mM; Sigma Aldrich). Since acetazolamide is a weak acid, the high concentration was solubilized in aCSF titrated to pH 9.0 (no additional buffer). Acetazolamide (45 mM; pKa, 7.2; 98% ionized at pH 9.0) added an excess of 89.1 $mOsm_C/L$; for pH 9.0, the solution of acetazolamide required 70 µL/mL of 0.5 N NaOH, which contributed an additional 70 $mOsm_C/L$. Because of the high osmolarity of the acetazolamide infusion solution, the effect of a solution of mannitol (88.2 mM, pH 9.0) in aCSF which, for pH 9.0, required 0.66 µL/mL of 0.5 N NaOH was studied as a control.

Procedure for validating aqueduct occlusion

Intraventricular infusion of hematoxylin and eosin (H&E) was used to check the integrity of the block of the aqueduct by mineral oil. In 3 rats, the aqueduct was occluded using mineral oil, as described above. In another 3 rats, nothing was placed in the 4th ventricle, allowing for CSF outflow from both the cannulated lateral ventricle and from the 4th ventricle. In both groups, CSF exiting the lateral ventricle was measured as above, and in both groups, H&E-containing aCSF was infused into the contralateral ventricle as described above. H&E-containing aCSF was infused at a nominal rate of 2 µL/min for 30 min. The rat then was euthanized by pentobarbital overdose, and was transcardially perfused with saline followed by 10% paraformaldehyde. In these cases, transcardial perfusion was performed with the rat’s head still held in the vertical orientation, to prevent loss of aqueductal occlusion and inadvertent spread of the H&E. These brains were embedded in OCT and frozen. The frozen block was photographed in the cryostat as it was cryosectioned to document the extent of H&E staining.

Data analysis

Numerical data are given as mean ± standard error of the mean (SE). Rates (µL/min) were calculated as the slope of the volume–time relationship, usually based on data collected over 30 min or more. Rates were determined for individual animals and were averaged across individuals of the same age. Calculations were performed using OriginPro (OriginLab Corporation, Northampton, MA).

Results

Aqueduct occlusion

CSF outflow from the cannulated lateral ventricle, without and with block of the aqueduct were compared. In the absence of block, the average rate of CSF outflow in 3 rats over the course of 1 h was 0.20 µL/min (Fig. 2A). In the same rats, blocking the aqueduct with mineral oil resulted in a 4-fold increase in the rate of outflow to 0.78 µL/min (9 weeks of age) (Fig. 2A). H&E staining of the ventricular system following intraventricular infusion of H&E, without and with block of the aqueduct were compared. In the absence of block, prominent staining was observed in the lateral ventricles, the aqueduct and 4th ventricle (Fig. 2B). By contrast, in rats with mineral oil block of the aqueduct, staining was observed in the lateral ventricles, as expected, but the 4th ventricle was unstained (Fig. 2C). This experiment confirmed that mineral oil placed in the vertically oriented 4th ventricle was highly effective in blocking the aqueduct. All subsequent experiments were carried out with mineral oil occlusion of the aqueduct. Next, the outflow pressure at which CSF was collected was examined for impact on the measured rate of CSF formation. For each rat, the effect of collecting CSF at 0, 1.5 and 3 cm of H_2O were compared. Rates of 0.76, 0.74 and 0.73 µL/min (9 weeks of age) were observed with outflow pressures of 0, 15 and 30 mm of H_2O, respectively (Fig. 2D). All subsequent experiments were carried out using outflow pressures of 0 mm H_2O.

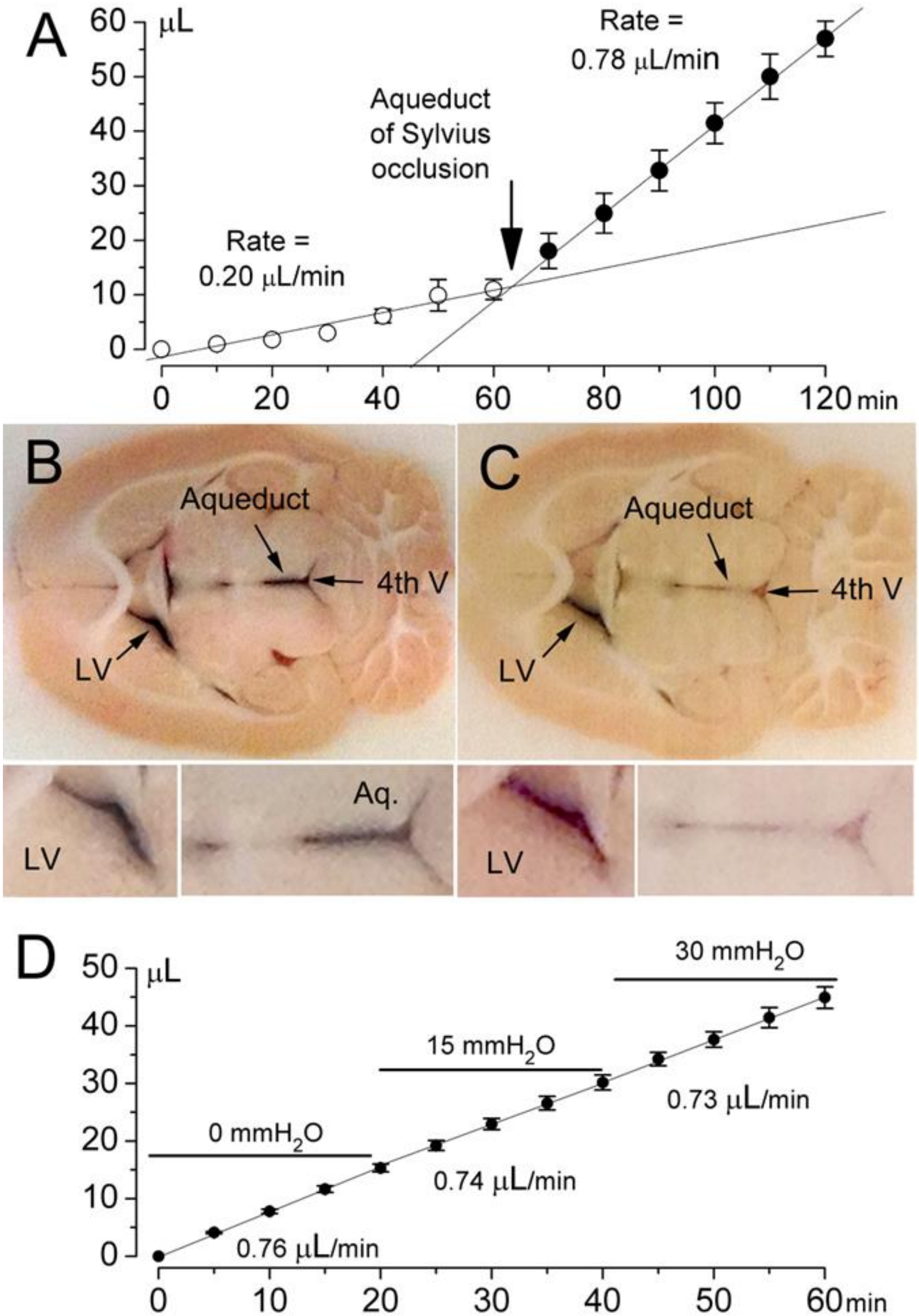
A
60
50
40
30
20
10
0
μL
Rate =
0.78 μL/min
Aqueduct
of Sylvius
occlusion
Rate =
0.20 μL/min
0
20
40
60
80
100
120 min
B
Aqueduct
4th V
LV
C
Aqueduct
4th V
LV
LV
Aq.
LV
D
50
40
30
20
10
0
μL
30 mmH2O
15 mmH2O
0 mmH2O
0.73 μL/min
0.74 μL/min
0.76 μL/min
0
10
20
30
40
50
60 min

Figure 2. The measured rate of CSF formation is increased by blockade of the Sylvian aqueduct but is not altered by increasing the outflow pressure

(**A**) CSF outflow from the left lateral ventricle was measured before and after occluding the 4th ventricle with mineral oil; before occlusion, the CSF outflow rate was 0.20 μL/min; after occlusion, the rate was 0.78 μL/min (3 rats; 9 weeks of age). (**B** and **C**) Hematoxylin and eosin (H&E) staining of the ventricular system without (**B**) and with (**C**) occlusion of the 4th ventricle with mineral oil; H&E dye was infused into the right lateral ventricle; the lateral ventricles (LV) were stained in both cases, but the aqueduct (Aq.) and 4th ventricle (4th V) were stained only in (**B**), not in (**C**); the data shown are representative of findings in 3 rats per condition. (**D**) CSF formation was measured at different outflow pressures; successive rates of 0.76, 0.74 and 0.73 μL/min (3 rats; 9 weeks of age) were observed with outflow pressures of 0, 1.5 and 3 cm of H2O, respectively.

Pharmacological inhibition of CSF formation

Studying CSF formation in real time during pharmacological inhibition requires intraventricular infusion of a drug solution at a known constant rate. This method was first evaluated by infusing aCSF. After cannulating the ventricle, the spontaneous rate of CSF formation was measured to be 1.16 µL/min (n = 3; 11 weeks of age) (Fig. 3A). Infusion of aCSF at the rate of 1.93 µL/min yielded a measured outflow rate of 2.98 µL/min, or a calculated rate of CSF formation 1.05 µL/min, which was within 10% of the baseline rate. CSF formation is dependent on carbonic anhydrase.[26, 30, 31] Therefore, to study the dynamic nature of this model, acetazolamide was used to inhibit CSF formation pharmacologically. Preliminary experiments showed that high concentrations of drug would have to be infused intraventricularly, likely due to the fact that active formation of CSF not only dilutes the infusate, but more importantly, it continuously washes drug away. Since acetazolamide is a weak acid, and since high concentrations of weak acids in aqueous solution are best obtained using basic pH, the drug infusion solution was titrated to pH 9.0. Infusion of acetazolamide (45 mM in aCSF; pH 9.0) decreased the calculated rate of CSF formation from 0.95 ± 0.23 to 0.48 ± 0.12 µL/min (n = 3; 10 weeks of age) (Fig. 3B). Inhibition of CSF formation by acetazolamide was not reversible, with a rate of 0.38 ± 0.10 µL/min measured during 30 min after cessation of drug infusion. The addition to aCSF of acetazolamide (45 mM) plus NaOH for pH 9.0 resulted in a large excess of osmols over that in aCSF alone.

Because CSF formation depends on the osmolarity of the compartment into which CSF is secreted, infusion of mannitol (88.2 mM in aCSF; pH 9.0) was used as a control. Infusion of the mannitol control solution increased the calculated rate of CSF formation from 0.96 ± 0.03 to 1.12 ± 0.17 μL/min (n = 3; 10 weeks of age) (Fig. 3B). The rate of CSF formation returned to 1.00 ± 0.12 μL/min, within 4% of the baseline value, after stopping the infusion. The observed increase in rate with mannitol likely reflected the increase in osmolarity due to the infusate,[41, 42] although additional experiments would be required to determine whether pH also had an effect. However, using this mannitol control infusion as baseline indicated that acetazolamide inhibited CSF formation by 57%, consistent with the overall process of CSF formation being highly dependent on HCO_3^-.[43]

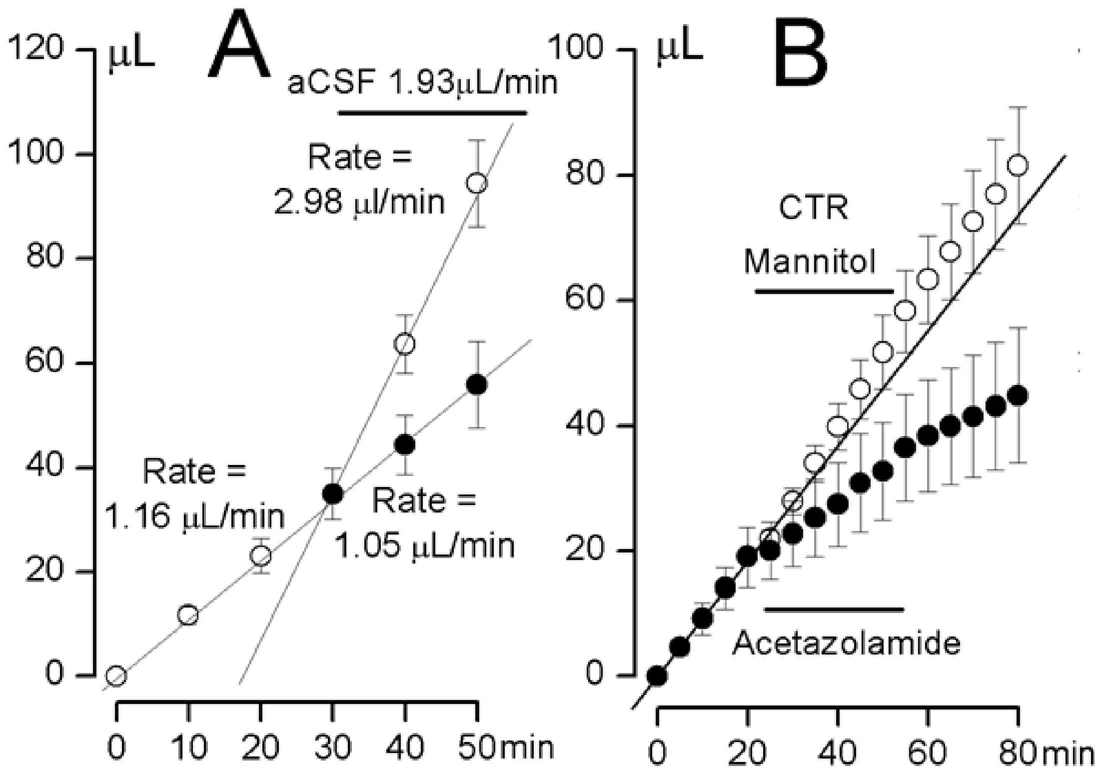

Figure 3. Pharmacological inhibition of CSF formation by acetazolamide.

(**A**) CSF out-flow at baseline was 1.16 µL/min; infusion of aCSF (1.93 µL/min) yielded a measured outflow rate of 2.98 µL/min, or a calculated rate of CSF formation of 1.05 µL/min, within 10% of baseline (3 rats; 11 weeks of age). (**B**) In two different experiments, CSF outflow at baseline was 0.95 ± 0.23 µL/min (filled circles) or 0.96 ± 0.03 µL/min(empty circles); infusion of acetazolamide (45 mM in aCSF; pH 9.0; 1.93 µL/min)or of mannitol (88.2 mM in aCSF; pH 9.0; 1.93 µL/min) yielded calculated rates of CSF formation 0.48 ± 0.12 µL/min (filled circles) or of 1.12 ± 0.17 µL/min (empty circles); based on these 2 experiments, inhibition by acetazolamide was calculated to be

57%; note that inhibition by acetazolamide was not reversible, with a rate of 0.38 ± 0.10 μL/min observed after stopping infusion (3 rats/experiment; 10 weeks of age).

CSF formation is age-dependent

In the forgoing experiments, baseline rates of CSF formation were occasionally different between groups, likely due to differences in age.[44, 45] Spontaneous CSF formation over the course of 60 min in rats of different ages were measured. The rates measured were 0.39 ± 0.06, 0.74 ± 0.05, 1.02 ± 0.04 and 1.40 ± 0.06 μL/min at 8, 9, 10 and 12 weeks, respectively (3 rats/group) (Fig. 4A and B).

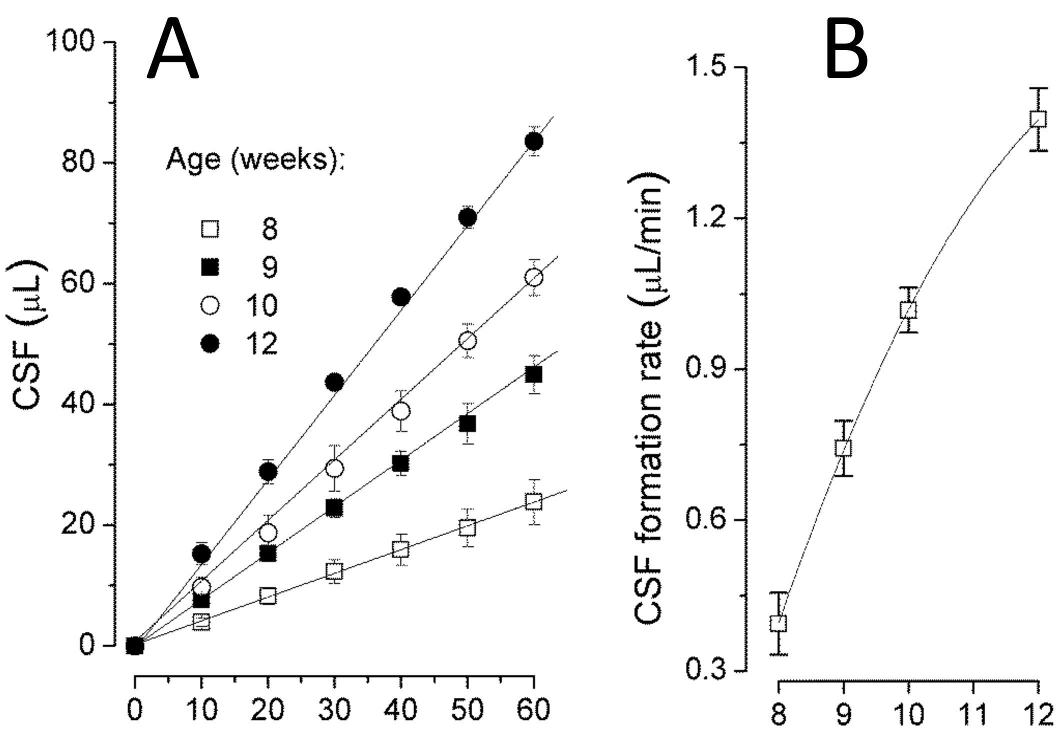

Figure 4. The effect of age on CSF formation
(**A**) CSF outflow at baseline was 0.39 ± 0.06, 0.74 ± 0.05, 1.02 ± 0.04 and 1.40 ± 0.06 μL/min at 8, 9, 10 and 12 weeks, respectively (3 rats/group). (**B**) Plot of the rate of CSF formation by the choroid plexus of the lateral ventricles as a function of age; data from (**A**).

Conclusions

The major finding of the present study is that we have developed a novel technique to perform direct real-time measurements of ongoing CSF formation by the brain of the rat in vivo. With this technique, it is feasible to study the effect of pharmacological manipulations on ongoing CSF formation. The method presented here is superior to the only other existing method in rodents, the tracer dilution method, which does not permit ongoing real-time determination of the rate of CSF formation, is not readily amenable to the study of pharmacological manipulations, and requires potentially confounding assumptions.

CHAPTER 3

SPAK-NKCC1 MEDIATED CSF HYPERSECRETION LEADS TO VENTRICULOMEGALY IN A MODEL OF IVH.

Materials and Methods

Animals

Animal experiments were performed under a protocol approved by the Institutional Animal Care and Use Committee (IACUC) of the University of Maryland, and in accordance with the guidelines and regulations in the NIH Guide for the Care and Use of Laboratory Animals. Male Wistar rats, age 8 weeks, (Harlan, Indianapolis, IN, USA), were anesthetized (60 mg/kg ketamine plus 7.5 mg/kg xylazine, IP) and allowed to breathe room air spontaneously. Body temperature was maintained at 37 ± 1°C (Harvard Apparatus, Holliston, MA, USA) throughout the course of the experiments.

IVH Model

IVH was modeled using a modified protocol based on previously described methods[15]. In an anesthetized animal, the tail artery was aseptically cannulated using a flexible catheter (PE-20) pre-loaded with heparinized saline. The rat was then mounted in a stereotactic apparatus (Stoelting Co., Wood Dale, IL), a midline scalp incision was made to expose the skull and a 1 mm burr hole was made using a high speed drill over the right lateral ventricle (coordinates, x= -0.8, y= -1.7 mm relative to bregma). Approximately 200 µL of blood was then drawn from the tail artery catheter and loaded into a 500 µL syringe (Hamilton, Reno, NV), which was then mounted to the stereotactic frame. Under stereotactic guidance, 50 µL of freshly collected autologous blood, free from anticoagulants, was infused into the right lateral ventricle (coordinates, x= -0.8, y= -1.7, z= -4.5 mm relative to bregma), over the course of 5 minutes, and the 26 gauge needle was held in place for an additional 20 minutes to prevent backflow of blood upon needle removal. Intraventricular infusion of sterile aCSF (Tocris, Bristol, UK) in the same manner served as the control condition.

Quantification of Rate of CSF Production

Rates of CSF production were measured as described in Chapter 2. Briefly, anesthetized rats were mounted in a stereotactic apparatus and a 1.3 mm burr hole was made over the left lateral ventricle (coordinates, x= -0.8, y= +1.7 relative to bregma). Next the rat's head was rotated on the ear-bars 90^{o}, nose-down, and the suboccipital muscles were dissected to the cisterna magna to expose the atlanto-occipital ligament. The ligament was punctured and a 23 gauge flexible catheter (PE-20) was advanced 5 mm through the foramen of Magendie to the 4th ventricle. Sterile, molecular grade mineral oil (100 µL; Sigma Aldrich, St. Louis, MO) was infused into the 4th ventricle to occlude the aqueduct of Slyvius, thereby creating a closed system of CSF circulation. With the rat in the same position, a glass capillary tube (cat # CV8010-300; borosilicate; OD, 1 mm; ID, 0.8 mm; length, 30 cm; VitroCom, Mountain Lakes, NJ) was advanced through the burr hole into the left lateral ventricle. The volume (V) of CSF that formed at a given timepoint was calculated as: $V\ (mm^3) = \pi \cdot r^2 \cdot d$, where r is the radius of the capillary tube and d is the distance CSF traveled within the capillary. Using the relationship $1\ mm^3 = 1\ \mu L$ the rate of CSF formation (µL/min) could be calculated from the slope of the volume–time relationship.

Ventricular Volume Analysis

Following IP injection of pentobarbital, rats were transcardially perfused with ice-cold normal saline followed by 10% neutral buffered formalin. The brains were harvested, kept in formalin for 24 hours at 4°C and then cryoprotected (30% sucrose). To prevent distortion from cryosectioning and slide mounting, we took high resolution pictures of serial coronal sections (200 µm apart, 14 levels) while the brain was mounted in the cryostat, using uniform parameters of camera positioning, magnification, and external lighting. Adobe Photoshop was used to obtain a pixel count of the lateral ventricles. Pixels were converted to area in mm^2, summed over 14 levels and multiplied by the distance between levels (0.2 mm) to calculate total ventricular volume.

8hr aCSF infusion

In an anesthetized naïve rat, a 28-gauge cannula from an Alzet brain infusion kit (#1; Durect, Cupertino, CA), with a single spacer to adjust the depth to 4.5 mm, was stereotactically placed in the burr hole over the right lateral ventricle and secured to the skull using cyanoacrylate adhesive. A solution of aCSF was infused at 1 µL/min over the course of 8 hours. At the end of 8 hours, the rat was euthanized and transcardially perfused and processed for ventricular volume analysis as described above.

Immunohistochemistry

Rats were transcardially perfused with ice-cold normal saline followed by 4% paraformaldehyde (PFA). Brains were harvested and kept in PFA for 24 hours before being transferred to a 30% sucrose solution for cryoprotection. Brains were cryosectioned (10µm, coronal), blocked (2% donkey serum, +0.2% Triton X-100 for 1 hour at RT) then incubated overnight at 4°C with primary antibodies. Sections were washed three times in phosphate-buffered saline and incubated for 1 hour at RT with secondary antibodies (1:500; Alexa Fluor 488 and Alexa Fluor 555; Invitrogen, Molecular Probes, Eugene, OR, USA). Sections were cover slipped using a polar mounting medium containing 4’6-diamidino-2-phenylindole (DAPI; Invitrogen, Eugene, OR, USA) and analyzed with epifluorescence microscopy (Nikon Eclipse 90i; Nikon Instruments Inc., Melville, NY, USA). Quantification was performed by regions of interest (ROI) using NIS-Elements AR software (Nikon Instruments Inc., Melville, NY, USA) and specific signal was defined as twice background.

Choroid plexus protein isolation and immunoblotting

Choroid plexuses were harvested rapidly from adult rat brains following transcardial perfusion with ice-cold saline. The brain was isolated and then placed in an ice-cold saline bath, after which the choroid plexus was carefully dissected under magnification using sharp forceps. Approximately 3 mg of choroid plexus tissue was harvested from one brain, which was then collected into a 1.5 mL tube. For western blot experiments, a strongly chaotropic lysis buffer (2% SDS, 8M urea, 14% sucrose, and 0.01% bromophenol blue) supplemented with freshly added protease and phosphatase inhibitor cocktail (PPI, Cell Signaling Technology, Danvers, MA) was added directly to the tube containing choroid plexus to reach an approximate final tissue concentration of 30 mg/mL. Crude lysate was incubated for an additional 10 minutes and then homogenized by centrifugation through a Qiashredder column (2 minutes, 6,000 RPM; Qiagen, Valencia, CA). Equal volumes of flow-through per condition were used directly for gel electrophoresis. Equal loading of total protein was assessed by reversible Ponceau S staining of membranes, as described previously.[46] Detection was performed using the ECL system (Amersham BioSciences Inc., Piscataway, NJ,) with routine imaging (Fuji LAS-3000) and quantification (ImageJ). Acquired data were normalized to total protein.

ICV Drug Treatment

The method described in Chapter 2 for administration of ICV drugs while measuring the rate of CSF secretion was used. Briefly, at the time of CSF collection, before rotating the head to a vertical orientation, a 28-gauge cannula from an Alzet brain infusion kit (#1; Durect, Cupertino, CA), with a single spacer to adjust the depth to 4.5 mm, was stereotactically placed in the burr hole over the right lateral ventricle and secured to the skull using cyanoacrylate adhesive. The cannula was connected via a preloaded PE-20 catheter to a 1 mL syringe containing the drug solution (see below). The syringe was loaded into a syringe infusion apparatus (Pump elite 11, Harvard Apparatus) and maintained at 37°C. To determine rate of CSF formation during intraventricular drug infusion, the "actual infusion rate" of the drug (1.93 µL/min) was subtracted from the "measured outflow rate" to obtain the "calculated rate of CSF formation". To assess the effect of a drug, the baseline rate of CSF formation was determined during spontaneous CSF formation (no drug infusion), then the calculated rate of formation was determined after switching to the test drug. Percent change (Δ%) was determined using the formula: $\Delta\% = \frac{(calculated\ rate) - (baseline\ rate)}{baseline\ rate}$. Intraventricular infusion solutions were made using artificial CSF (aCSF), composed as follows (in mM): Na 150; K 3.0; Ca 1.4; Mg 0.8; P 1.0; Cl 155, pH 7.19 (Tocris, Bristol, UK), with a calculated osmolarity of 311.2 mOsmC/L. The following drugs were used: acetazolamide (45 mM, pH 9; Sigma Aldrich, St. Louis, MO), STOCK-1S 50699 (100 µM, pH 6, 1% DMSO; a gift from Dr. Kristopher T. Kahle, a collaborating scientist), Closantel (30 µM, pH 7.2, 0.1% DMSO; Sigma Aldrich, St. Louis, MO), Bumetanide (2.7 mM, pH 9; Sigma Aldrich, St. Louis, MO). Due to differences in drug solubility, each drug had a specific vehicle control to account for pH, DMSO co-solvent, and osmolarity to ensure that these differences did not alter rate of CSF production. For each control solution, aCSF solution was altered using NaOH and HCl (Sigma Aldrich, St. Louis, MO), to adjust pH, and mannitol (Sigma Aldrich, St. Louis, MO), to adjust the osmolarity. In each case, the vehicle controls had no statistical effect on the baseline rate of CSF and therefore, a representative vehicle control will be presented in data analysis for simplicity of data presentation.

In vivo knockdown of SPAK

Previously validated SPAK antisense oligodeoxynucleotides (ODN; Integrated DNA Technologies, Coralville, IA) were used for in vivo knockdown of SPAK.[47] ODNs were reconstituted in sterile normal saline and diluted to a final concentration of 0.5 µg/µL for ICV injection. All solutions were sterile filtered. The rats were injected ICV under stereotactic guidance with a 10 µL bolus of either SPAK or scrambled ODN every 12h starting 24h prior to IVH and continued until 48hr following IVH. The sequences were as follows:

SPAK, GG*CTCC*GCC*ATG*ATGC*TGC;

Scrambled, CGC*TCG*ATCC*AGG*TCA*GCG (* denotes position of locked nucleic acids). To validate the ODNs ability to knockdown SPAK, IHC was used to detect SPAK and pNKCC1 in Naïve and 24hr IVH with either scrambled or anti-SPAK ODN.

Antibodies for IHC and Western Blot

The following primary antibodies were used: rabbit anti-SPAK (1:2000; Cell Signaling Technology); rabbit anti-phosphorylated SPAK (pSPAK, Ser 373, 1:2,000, EMD Millipore, Billerica, MA); rabbit anti-NKCC1 (1:2,000, Abcam, Cambridge, MA); rabbit anti-phosphorylated NKCC1 (pNKCC1, Thr 212/Thr 217, 1:2,000, EMD Millipore). Protein was detected using species appropriate HRP-tagged secondary antibodies (Cell Signaling Technology).

Data Analysis

All statistics were completed in OriginPro (OriginLab Corporation, Northampton, MA) using one-way ANOVA analysis with a Tukey post-hoc test for differences between groups. Numerical data are given as mean ± standard error of the mean (SE). Rates (µL/min) were calculated as the slope of the volume-time relationship, based on data collected over 30 min or more. Rates were determined for individual animals and were averaged across individuals.

Results

IVH increases rate of CSF Production and is sufficient to produce ventriculomegaly

Rates of CSF production were measured 48 hours after the onset of IVH and compared to age-matched controls. The rate of CSF production in the IVH group was ~3-fold higher than the naïve controls (1.43 ± 0.07 µL/min versus 0.45 ± 0.05 µL/min, respectively, n=13, 10, $p<0.01$ IVH versus naïve) (Fig. 5A). H&E staining (Fig. 5B) and volumetric analysis (Fig. 5C) demonstrated that ventriculomegaly was present 48 hours after IVH versus naïve and vehicle groups [ventricular volume (mm^3): 5.39 ± 0.74, 1.94 ± 0.08, and 2.45 ± 0.07, respectively; n=3, $p<0.01$ IVH versus naïve and vehicle]. To directly evaluate whether IVH-associated CSF hypersecretion contributes to ventriculomegaly, aCSF was infused into the right lateral ventricle of naïve rats for 8 hours at a rate of 1 µL/min, approximately the difference observed in rates of CSF secretion between rats subjected to IVH and naive controls. An 8-hour infusion of aCSF resulted in increases in ventricular volume (4.90 ± 0.41 mm^3, n=5) that was increased significantly versus controls but not significantly different than IVH ($p<0.01$ versus naïve and vehicle; $p>0.05$ versus IVH) (Fig. 5B, C).

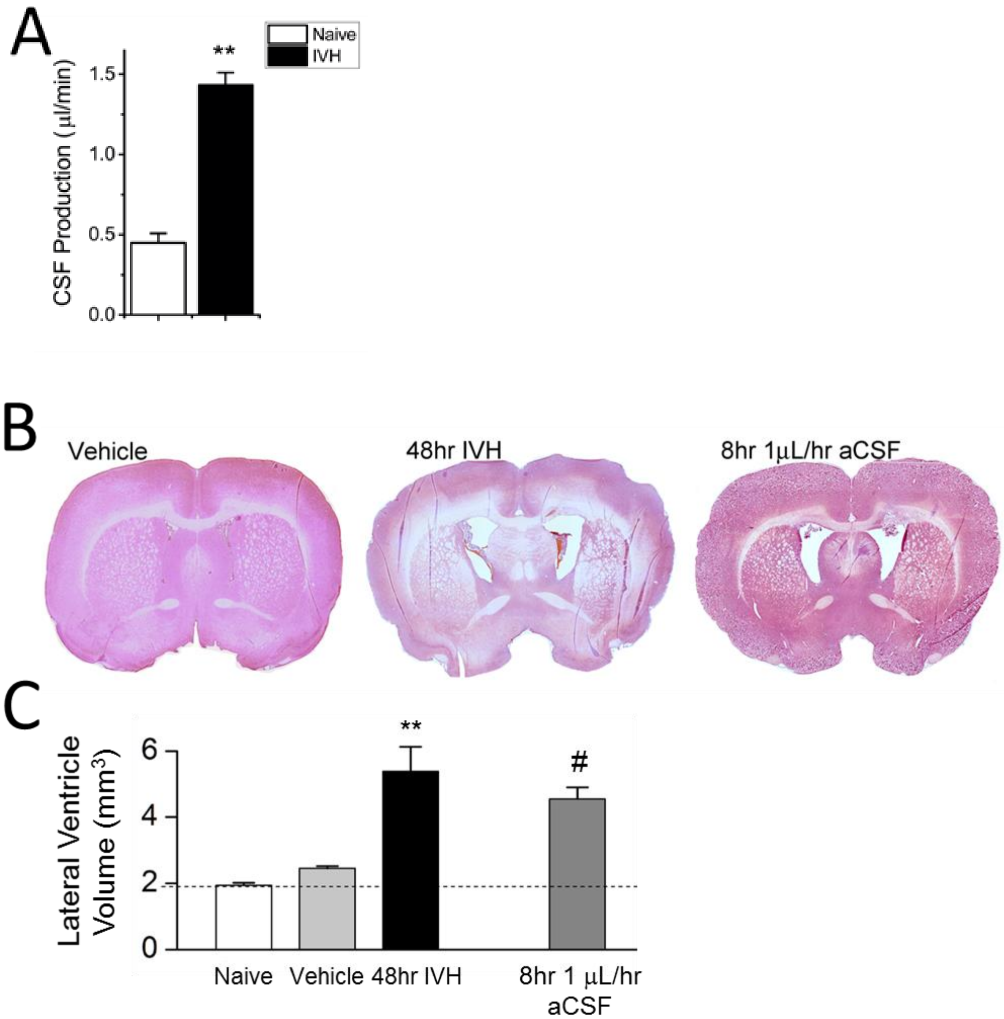
A
CSF Production (μl/min)
1.5
1.0
0.5
0.0
**
Naive
IVH
B
Vehicle
48hr IVH
8hr 1μL/hr aCSF
C
Lateral Ventricle Volume (mm3)
6
4
2
0
**
#
Naive
Vehicle
48hr IVH
8hr 1 μL/hr aCSF

Figure 5. IVH induces ventriculomegaly through increased CSF production

Rats subjected to a model of IVH were studied. IVH, 50 µL autologous blood injection; Vehicle, 50 µL aCSF injection; 8hr 1 µL/hr aCSF, continuous infusion of aCSF into lateral ventricles at 1µL/hr for 8 hours. **(A)** Rates of CSF production (µL/min) in Naïve and 48 hr IVH groups (Age 8 weeks; at least 10 rats per group). **(B)** H&E stains of coronal brain cryosections from Naïve, Vehicle, 48 hr IVH and 8hr continuous aCSF infusion groups, and quantification of ventricular volume (mm^3) in (**C**). **, $p<0.01$; #, $p>0.05$ versus IVH and $p<0.01$ versus naïve and vehicle.

NKCC1 is a key player in hypersecretion of CSF

Both NKCC1 and carbonic anhydrase (CA) are involved in CSF production.[26, 40] In order to determine whether NKCC1 or CA mediated IVHH, pharmacological inhibitors bumetanide, a selective inhibitor of NKCC1 activity, and acetazolamide, a CA inhibitor, were infused ICV 48 hours after IVH at the time CSF secretion rates were measured. Bumentanide inhibition of NKCC1 reduced the rate of CSF secretion in IVH rats by ~83% compared to ICV vehicle infusion (0.24 ± 0.11 μL/min versus 1.41 ± 0.26 μL/min, respectively, n=3) ($p<0.01$ bumetanide versus vehicle). In contrast, acetazolamide inhibition of CA reduced the rate of CSF secretion in IVH rats by ~18%, compared to ICV vehicle infusion (1.16 ± 0.14 μL/min versus 1.41 ± 0.26 μL/min, n=3) ($p>0.05$ acetazolamide versus vehicle).

These data demonstrate that NKCC1, not CA, is a key player in IVH-induced hypersecretion of CSF.

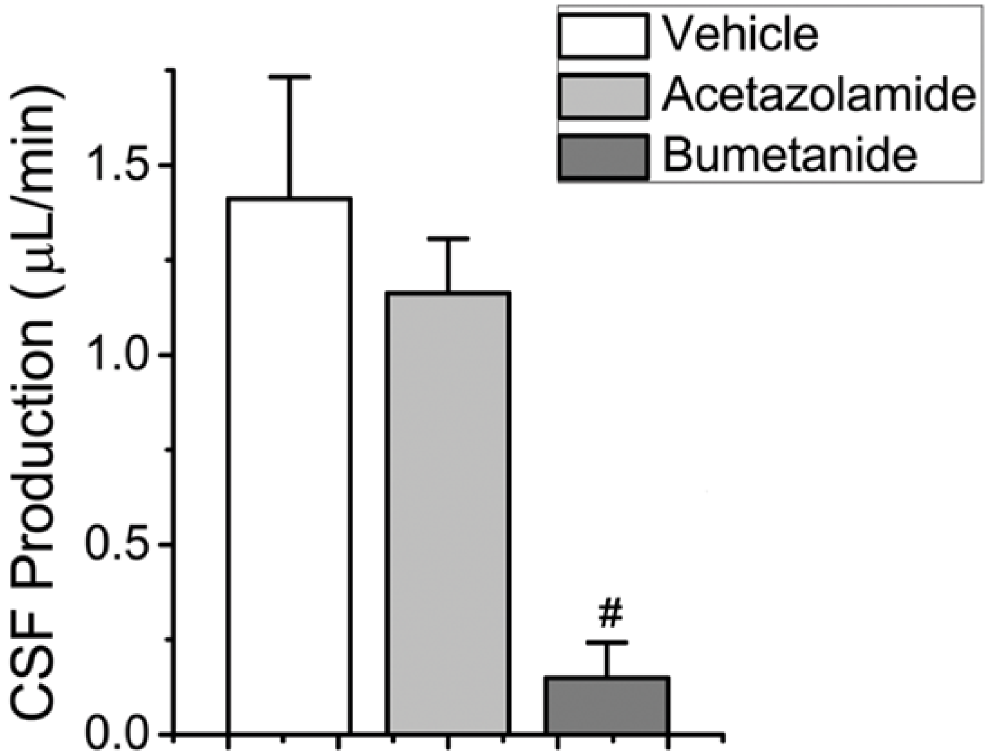

Figure 6. NKCC1 regulates CSF production in IVHH.
Rates of CSF production with concurrent ICV infusion of drugs were measured in rats 48 hours after IVH. Vehicle infusion was adjusted to match the osmolarity of each drug. Acetazolamide, 45 mM, 88.2 mOsm, pH 9; bumetanide, 2.7 mM, 8.1 mOsm, pH 9; vehicle, 88.2 mM, 88.2 mOsm, pH 9, mannitol-aCSF solution. #, $p<0.01$ versus vehicle and acetazolamide.

SPAK and NKCC1 are phosphorylated following IVH.

Once NKCC1 was shown to be a potential molecular target to attenuate IVH-induced CSF hypersecretion, regulation of NKCC1 was considered. In other secretory epithelial systems, NKCC1 activity is regulated by direct phosphorylation via the kinase SPAK.[33, 48, 49] Additionally, SPAK activity is also regulated via phosphorylation. Thus, the phosphorylation states of both NKCC1 and SPAK were studied following IVH via quantitative immunohistochemistry (IHC) and western blot analysis.

Quantification (via percent region of interest analysis) of immunolabeled coronal brain cryosections indicated SPAK and NKCC1 are phosphorylated at the apical membrane of the CPE 48 hours following IVH. Phospho-SPAK (pSPAK) increased 2-fold 48 hours after IVH compared to vehicle (36.95 ± 3.49%, versus 17.91 ± 4.57%, respectively, n=4) ($p<0.01$ IVH versus vehicle). Phospho-NKCC1 (pNKCC1) increased 8-fold 48 hours after IVH compared to vehicle (20.21 ± 1.86 % versus 2.58 ± 0.62 %, respectively, n=4) ($p<0.01$ IVH versus vehicle) (Figure 7A).

Western blot analysis of freshly isolated CPE tissue corroborated the finding that SPAK and NKCC1 were phosphorylated 48 hours following IVH. pSPAK was increased 1.5-fold 48 hours after IVH compared to vehicle and ~2-fold compared to naïve control (reported in arbitrary units: 2.43 ± 0.32 versus 1.65 ± 0.24 versus 1.31 ± 0.15, respectively, n=7, 6, 7) ($p<0.05$, IVH versus; $p<0.01$ IVH versus naive). pNKCC1 was increased ~2-fold 48 hours following IVH compared to vehicle and 5-fold compared to naïve control (reported in arbitrary units: 1.07 ± 0.12 versus 0.55 ± 0.14 versus 0.20 ± 0.03, respectively, n=5 all groups). Western blot analysis of the same samples showed there was no significant difference in quantity of total SPAK or NKCC1 protein.

Taken together, these data show that IVH induces the activation SPAK and NKCC1 via phosphorylation.

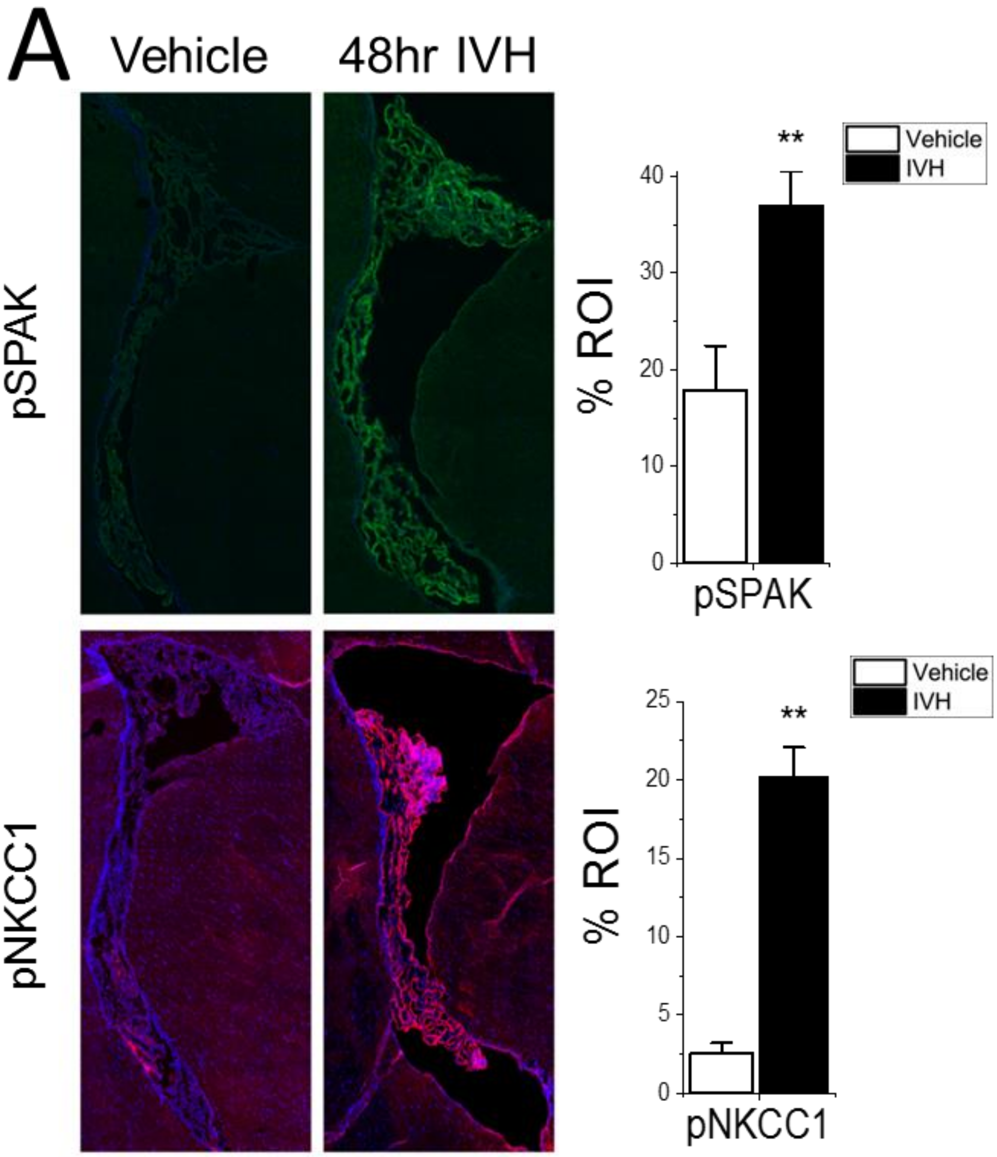
A
Vehicle
48hr IVH
pSPAK
pNKCC1
Vehicle
IVH
**
% ROI
40
30
20
10
0
pSPAK
Vehicle
IVH
**
% ROI
25
20
15
10
5
0
pNKCC1

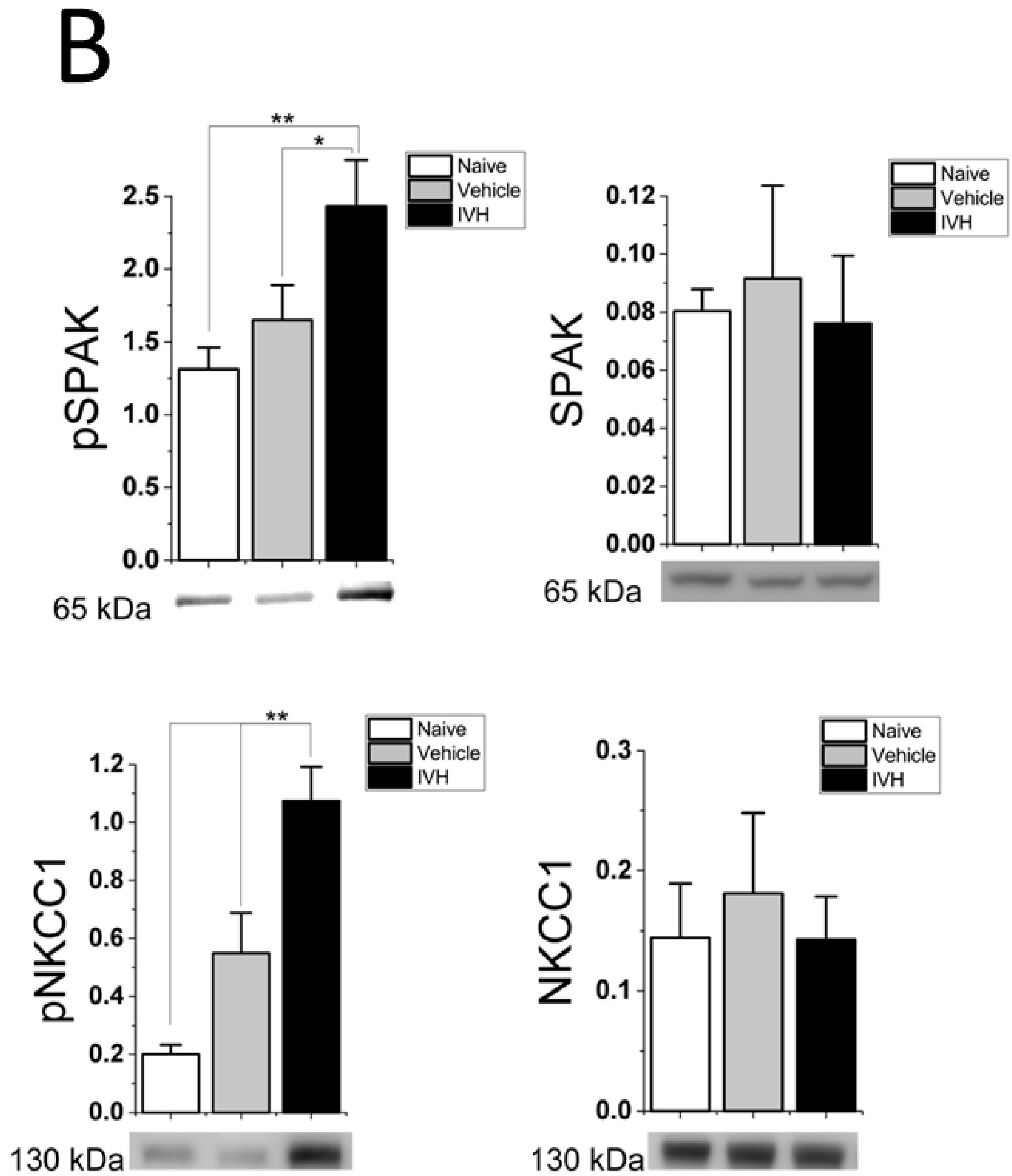

Figure 7. SPAK and NKCC1 are phosphorylated in response to IVH.
(**A**) Region of interest (ROI) quantification of immunohistochemistry. IVH, 50 μL autologous blood, 48 hrs following injection; vehicle, 50 μL aCSF, 48 hrs following injection; n=4 per group. (**B**) Western blot analysis, measured in arbitrary units, at least 5 animals per group. *, p<0.05; **, p<0.01.

Knockdown of SPAK prevents phosphorylation of NKCC1 and attenuates CSF hypersecretion following IVH

SPAK is a kinase known to phosphorylate NKCC1 in other epithelial tissues. After the finding that SPAK and NKCC1 are phosphorylated following IVH, antisense oligodeoxynucleotides (ODNs) to target SPAK were used to determine if IVH induces phosphorylation of NKCC1 via a SPAK-dependent mechanism.

Immunolabeling of coronal cryosections demonstrate that in the naïve rat SPAK is ubiquitously expressed in the CPE and that NKCC1 is not phosphorylated (Figure 8A, D). Scrambled ODNs did not have any effect on presence of SPAK and NKCC1 was phosphorylated following IVH (Figure 8B, E). SPAK-ODNs were able to successfully knockdown SPAK and prevent IVH-induced phosphorylation of NKCC1 (Figure 8C, F).

In a separate group of rats, the same protocol for ODN administration and IVH was performed and the rate of CSF production was measured 48 hours after IVH. SPAK antisense decreased the rate of CSF production ~50% compared to the scrambled ODN (0.62 ± 0.08 µL/min versus 1.20 ± 0.13 µL/min, respectively, n=5) ($p<0.01$) (Figure 9A).

These experiments indicate that SPAK phosphorylates NKCC1 in the CPE after IVH. Additionally, knockdown of SPAK is a viable method of decreasing IVH-induced CSF hypersecretion.

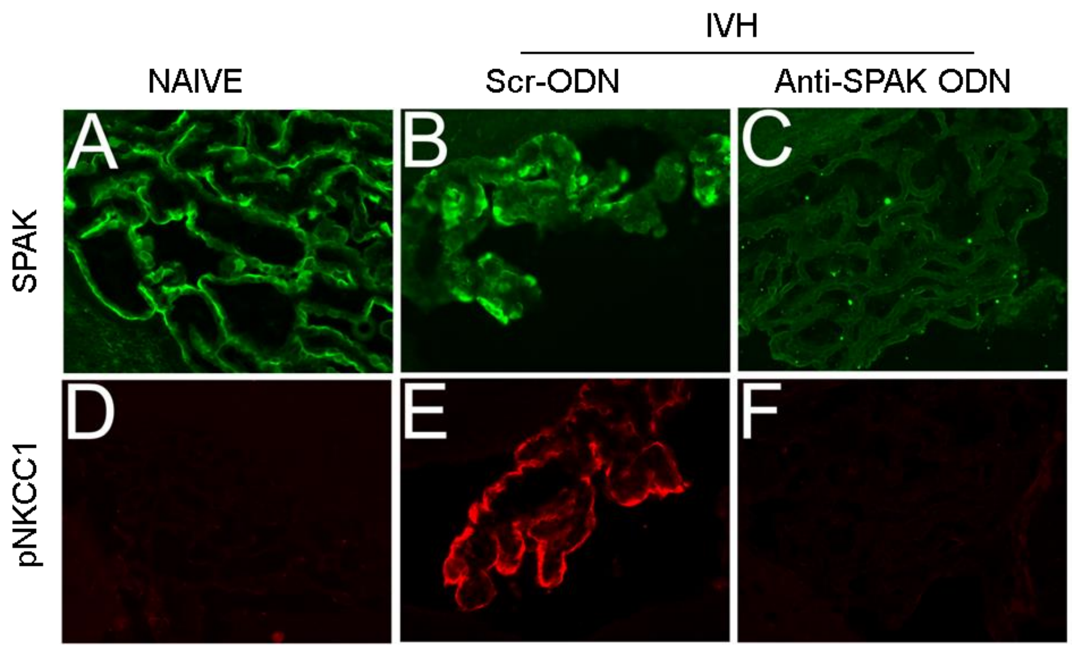

Figure 8. Knockdown of SPAK via Antisense ODN Prevents Phosphorylation of NKCC1 Following IVH.

Immunohistochemistry of choroid plexus. (A-C) SPAK (green). (D-F) Red, pNKCC1. (A) SPAK is ubiquitously expressed in the choroid plexus. (B) SPAK levels are not effected following scrambled ODN injections at 24 hrs following IVH. (C) SPAK is knocked down with anti-SPAK ODN injections following 24 hrs IVH. (D). NKCC1 is not phosphorylated in a naïve animal. (E) NKCC1 is phosphorylated 24 hrs following IVH with scrambled ODN injections. (F) NKCC1 is not phosphorylated 24 hrs following IVH with anti-SPAK ODN injections.

Pharmacological inhibition of SPAK attenuates CSF hypersecretion and prevents ventriculomegaly

In addition to ODNs, other measures for preventing SPAK-mediated phosphorylation of NKCC1 following IVH were sought after. Recently, two drugs, STOCK1S-50699 and closantel, have been shown to inhibit SPAK.[50-52]

STOCK1S-50699 and closantel were infused ICV at the time of CSF rate measurement. STOCK1S-50699 decreased rates of CSF production by ~50% compared to vehicle control (0.70 ± 0.08 µL/min versus 1.41 ± 0.26 µL/min, respectively, n=3) (Figure 9A; $p<0.01$ STOCK1S-50699 versus vehicle). Closantel decreased rates of CSF production by ~66% compared vehicle control (0.48 ± 0.08 µL/min versus 1.41 ± 0.26 µL/min, respectively, n=3) (Figure 9A; $p<0.01$ closantel versus vehicle).

The effect of closantel on IVH-induced ventriculomegaly was determined by continuous ICV infusion of closantel via an osmotic pump at the onset of IVH. Ventriculomegaly was decreased by ~43 with closantel treatment compared to IVH and was not statistically different from vehicle [ventricular volume (mm^3): 3.08 ± 0.28, 5.39 ± 0.74, 2.45 ± 0.07, respectively, n=3) ($p<0.05$ closantel versus IVH, $p>0.05$ closantel versus vehicle)] (Figure 9B, C).

These data demonstrate that pharmacological inhibition of SPAK attenuates CSF hypersecretion, which significantly reduces IVHH.

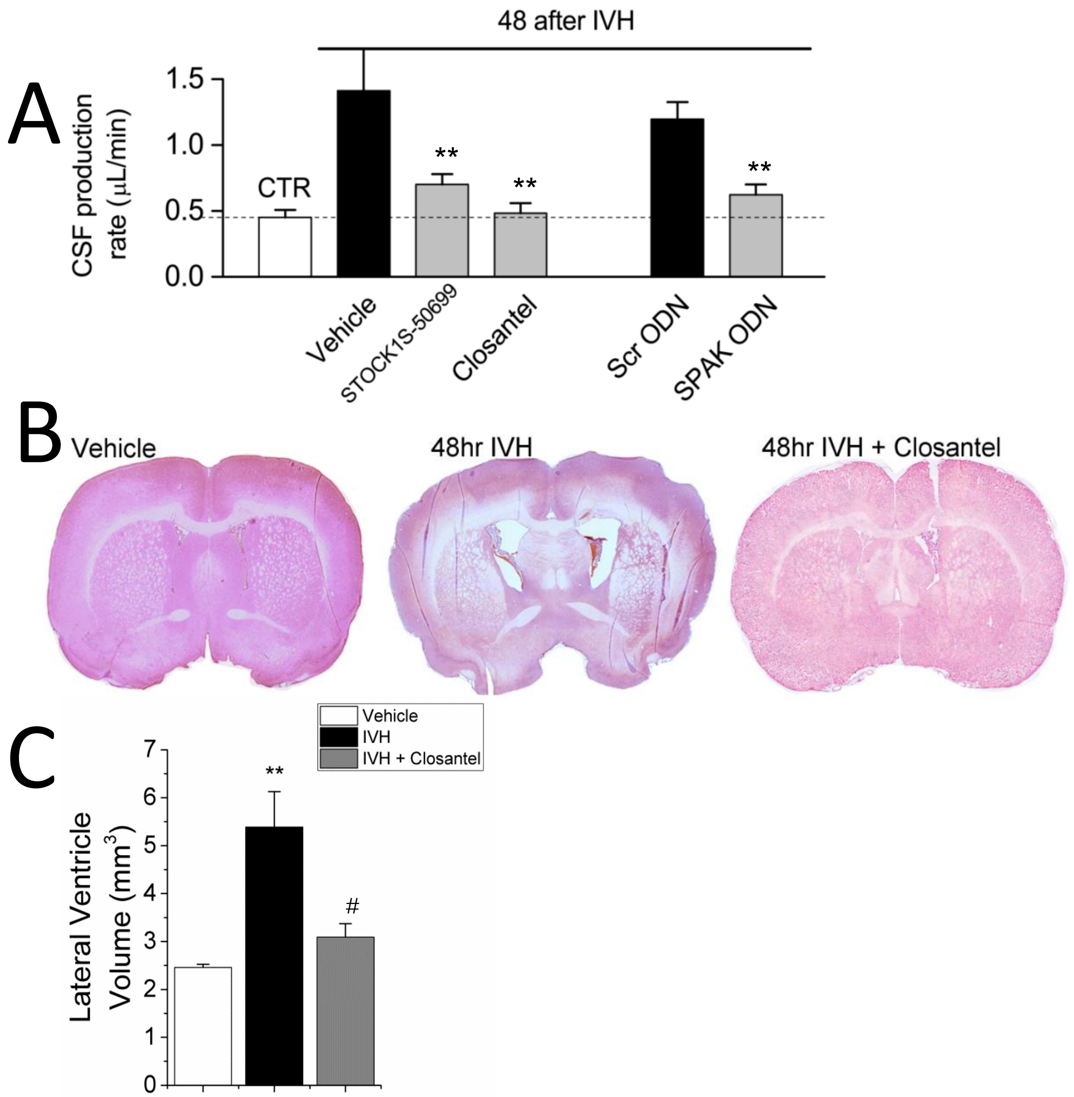
A
48 after IVH
CSF production rate (μL/min)
1.5
1.0
0.5
0.0
CTR
**
**
**
Vehicle
STOCK1S-50699
Closantel
Scr ODN
SPAK ODN
B
Vehicle
48hr IVH
48hr IVH + Closantel
C
Vehicle
IVH
IVH + Closantel
Lateral Ventricle Volume (mm³)
7
6
5
4
3
2
1
0
**
#

Figure 9. Inhibition of SPAK prevents IVHH.

(**A**) Rates of CSF production with concurrent ICV vehicle, aCSF, pH 6; STOCK1S-50699, 100 µM, pH 6, 1% DMSO; closantel, 30 µM, pH 7.2; 3 animals per group or continuous ICV infusion via osmotic pump, Scr and SPAK ODN, 10 µg/day; 5 animals per group, were measured in rats 48 hours after IVH. (**B**) H&E stain of vehicle, 50µL aCSF injection; 48 hr IVH, 50µL autologous blood injection; 48hr IVH + closantel, 50µL autologous blood injection plus continuous ICV closantel infusion via osmotic pump. (**C**) Ventricular volume analysis of vehicle, IVH and IVH + closantel groups in B, 3 animals per group. **, $p<0.01$ versus vehicle. #, $p<0.05$ versus IVH.

Conclusions

There are three novel findings from this set of experiments: (i) IVH increases the rate of CSF production, which is sufficient to produce ventriculomegaly; (ii) NKCC1 is phosphorylated by SPAK in response to accumulation of blood in the ventricles; (iii) Multiple methods of targeting SPAK can lower rates of CSF production and subsequent ventriculomegaly.

CHAPTER 4

DISCUSSION

There are five novel findings presented in this thesis: (i) it is possible to directly measure the rate of CSF production in rats under near-physiological conditions; (ii) pharmacological agents can be administered ICV without confounding measurement of CSF production rate; (iii) IVH increases the rate of CSF production, i.e. CSF hypersecretion; (iv) phosphorylation of NKCC1 drives CSF hypersecretion in response to a model of IVH; (v) inhibiting SPAK reduces phosphorylation of NKCC1, lowers rates of CSF production after IVH, and attenuates IVH associated ventriculomegaly.

The development of a new method to study CSF dynamics in rats was crucial to the advancement of this project. Eight distinct methods have been described for measuring CSF formation in vivo[39], which include the direct methods, wherein the rate of CSF production is directly measured, and the indirect methods, wherein the rate of CSF production is inferred based on another marker. All of the direct methods require the use of highly non-physiological conditions, such as removing brain tissues overlying the choroid plexus and collecting CSF under oil,[39, 53] removing CSF from the ventricle and observing the time needed to refill the ventricle,[54] or extracorporeal perfusion of the choroid plexus.[39, 55] The indirect methods, which include tracer dilution, and MRI, require one or more assumptions that may be difficult to justify.[39] Thus, none of the 8 methods described to date is readily suited for quantifying CSF formation in laboratory rodents *in vivo*, in real-time, under near-physiological conditions.

Prior to the method described in chapter 1,[40] there were no published models that allowed for the measurement of CSF production while simultaneously introducing an ICV therapeutic. In clinical trials, therapeutic options have failed simply because the drug cannot cross the blood-brain barrier (BBB) – not because the drug is ineffective.[56-59] For example, in 2015, a clinical trial using bumetanide, administered systemically, as an add-on treatment for neonatal epilepsy was found ineffective.[60] However, another group demonstrated that a BBB permeable bumetanide prodrug BUM5, was effective in a mouse model of epilepsy.[61] These studies demonstrate that the efficacy of a drug can be dependent on route of administration; therefore, it is important for preclinical research targeting the brain to consider BBB permeability. Indeed, pilot studies of this project, no change in CSF secretion was observed when bumetanide, a BBB impermeable agent,[60, 61] was administered systemically (data not shown), however, ICV infusion of bumetanide yielded an 83% decrease in the rate of CSF production. Thus, the model described in Chapter 1 is impactful in that it allows for the study effects of systemic and direct CNS drug administration on the rate of CSF production and should prove useful for studying many other diseases effecting CSF dynamics.

The predominant view of IVHH is that blockages in arachnoid granulations impair reabsorption of CSF, resulting in a pathological accumulation of CSF in the ventricular system.[6, 14] However, the results presented in this thesis, that rats submitted to IVH exhibit a nearly 3-fold increase CSF production rate and ventriculomegaly 48 hours after IVH, suggest that IVHH may be partially or mostly driven by increased CSF production. Interestingly, hydrocephalus that manifests during other pathologies has also been linked to increased CSF production. For example, choroid plexus pathologies such as papilloma and villous hypertrophy are known to generate increased CSF secretion rates, resulting in hydrocephalus.[62, 63] Case reports of hydrocephalic patients with choroid plexus papilloma or villous hypertrophy estimate a 4 to 5 fold increase in CSF production.[21, 23, 64, 65]

Carbonic anhydrase, a CPE enzyme, converts H_2O and CO_2 into H^+ and HCO_3^-, providing HCO_3^- needed for the Na^+/ HCO_3^- transporters involved in CSF formation. In Chapter 2, as a part of validating the new method of measuring rates of CSF production, acetazolamide was infused ICV into naïve rats and decreased rates by 57%. This value is corroborated in the literature as patients and laboratory animals treated with acetazolamide generally have a ~30 to 50% decrease in CSF rate and daily output[66-68]. However, in rats with IVH, ICV acetazolamide decreased CSF the production rate by a modest 18%, which was not significantly different than vehicle infusion. These data indicate that the increased rate of CSF production following IVH is not driven by carbonic anhydrase activity.

NKCC1 is an electroneutral ion co-transporter that is found in almost all secretory epithelia in the body. NKCC1 acts to maintain the osmotic gradients of Na^+, K^+ and Cl^- across the CPE for proper movement of water. When NKCC1 was inhibited by ICV bumetanide, in rats with IVH, a robust 83% decrease in CSF rate was observed. Previous laboratory studies have shown that bumetanide is effective in decreasing CSF[69, 70], although, not to the extent that presented here. This could be due to (i) the use cell culture not able to perfectly model an in vivo system, or (ii) the tracer dilution method used to measure rates, which can have an effect on osmolarity and skew results.[39, 41, 42] These results taken together suggest that NKCC1, and not carbonic anhydrase, has an important role in increased rates of CSF production following IVH.

Results of immunohistochemistry and western blot analysis indicate increased phosphorylation of SPAK and NKCC1 following IVH. In other organ systems, phosphorylation increases SPAK activity and NKCC1 turnover rates.[33, 48, 49] As a proof of concept, ODNs directed at SPAK were implemented and indicated that, in the knockdown of SPAK, IVH-induced pNKCC1 and CSF hypersecretion were attenuated. For the first time in he CPE, a SPAK-NKCC1 axis driving IVH-induced CSF hypersecretion has been defined. The SPAK-NKCC1 axis offers new molecular targets for minimally invasive treatment of IVHH.

SPAK ODNs are useful tools for characterizing molecular pathways; however, they are not suitable for treatment in a clinical setting. Therefore, other SPAK inhibiting compounds were studied. Recently, SPAK inhibitors, such as STOCK1S-50699 and closantel, have been utilized in SPAK-associated diseases, such as hypertension and Gordon’s Syndrome[50-52]. Here, both compounds decreased the magnitude of IVH-induced CSF hypersecretion, similar to that of transcriptional inhibition via SPAK ODNs. Notably, closantel had the largest effect on secretion rate among the SPAK inhibitors tested and ventriculomegaly was significantly decreased after 48 hr IVH. These data have significant clinical implications because ventriculomegaly, the hallmark of hydrocephalus, can be prevented using minimally invasive pharmacological treatment. Overall, these results suggest the possibility that an add-on drug at the time of an EVD or VP shunt could improve patient outcomes, via decreased CSF hypersecretion, with IVHH.

Future studies will need to address the time course of IVH-induced CSF hypersecretion. The data presented in this thesis is focused on 48 hours after IVH. However, it is possible that CSF hypersecretion, although sufficient to produce ventriculomegaly acutely after IVH, is transient and other factors leading to hydrocephalus are involved. For example, Rekate et. al, tested the hypothesis that CSF hypersecretion via choroid plexus papilloma leads to hydrocephalus[24]. The study infused aCSF into the ventricles to simulate CSF hypersecretion, in mongrel dogs that had kaolin-induced hydrocephalus and naïve controls. They found that CSF hypersecretion increased ventricular volume in the naïve dog, but ventriculomegaly was exacerbated by restricted CSF flow via kaolin-injection. These results, and those presented herein,suggest the possibility that CSF hypersecretion and impaired reabsorption may both contribute to IVHH. Thus, the time course of CSF hypersecretion will be important in understanding how therapeutics can be implemented.

These data suggest that activation of the SPAK-NKCC1 pathway leads to CSF hypersecretion is and drives the pathogenesis of IVHH. Pharmacological inhibitors that target the SPAK-NKCC1 may effectively prevent CSF hypersecretion and IVHH. These findings hold strong potential for pharmacological alternatives to the current invasive surgical methods used to treat IVHH.

References List

1. Mozaffarian D, Benjamin EJ, Go AS, et al: Executive Summary: Heart Disease and Stroke Statistics-2016 Update: A Report From the American Heart Association. **Circulation 133**:447-454, 2016

2. Sidney S, Rosamond WD, Howard VJ, et al: The "heart disease and stroke statistics--2013 update" and the need for a national cardiovascular surveillance system. **Circulation 127**:21-23, 2013

3. Hanley DF: Intraventricular hemorrhage: severity factor and treatment target in spontaneous intracerebral hemorrhage. **Stroke 40**:1533-1538, 2009

4. Hinson HE, Hanley DF, Ziai WC: Management of intraventricular hemorrhage. **Curr Neurol Neurosci Rep 10**:73-82, 2010

5. Coplin WM, Vinas FC, Agris JM, et al: A cohort study of the safety and feasibility of intraventricular urokinase for nonaneurysmal spontaneous intraventricular hemorrhage. **Stroke 29**:1573-1579, 1998

6. Kahle KT, Kulkarni AV, Limbrick DD, Jr., et al: Hydrocephalus in children. **Lancet 387**:788-799, 2016

7. Steiner T, Diringer MN, Schneider D, et al: Dynamics of intraventricular hemorrhage in patients with spontaneous intracerebral hemorrhage: risk factors, clinical impact, and effect of hemostatic therapy with recombinant activated factor VII. **Neurosurgery 59**:767-773, 2006

8. Badhiwala JH, Hong CJ, Nassiri F, et al: Treatment of posthemorrhagic ventricular dilation in preterm infants: a systematic review and meta-analysis of outcomes and complications. **J Neurosurg Pediatr**1-11, 2015

9. Tamber MS, Klimo P, Jr., Mazzola CA, et al: Pediatric hydrocephalus: systematic literature review and evidence-based guidelines. Part 8: Management of cerebrospinal fluid shunt infection. **J Neurosurg Pediatr 14 Suppl 1**:60-71, 2014

10. Khan F, Rehman A, Shamim MS, et al: Factors affecting ventriculoperitoneal shunt survival in adult patients. **Surg Neurol Int 6**:25, 2015

11. Spader HS, Hertzler DA, Kestle JR, et al: Risk factors for infection and the effect of an institutional shunt protocol on the incidence of ventricular access device infections in preterm infants. **J Neurosurg Pediatr 15**:156-160, 2015

12. Gaberel T, Magheru C, Emery E: Management of non-traumatic intraventricular hemorrhage. **Neurosurg Rev 35**:485-494, 2012

13. Strahle J, Garton HJ, Maher CO, et al: Mechanisms of hydrocephalus after neonatal and adult intraventricular hemorrhage. **Transl Stroke Res 3**:25-38, 2012

14. Cherian S, Whitelaw A, Thoresen M, et al: The pathogenesis of neonatal post-hemorrhagic hydrocephalus. **Brain Pathol 14**:305-311, 2004

15. Simard PF, Tosun C, Melnichenko L, et al: Inflammation of the choroid plexus and ependymal layer of the ventricle following intraventricular hemorrhage. **Transl Stroke Res 2**:227-231, 2011

16. Thiagarajah JR, Donowitz M, Verkman AS: Secretory diarrhoea: mechanisms and emerging therapies. **Nat Rev Gastroenterol Hepatol 12**:446-457, 2015

17. Aikawa T, Shimura S, Sasaki H, et al: Marked goblet cell hyperplasia with mucus accumulation in the airways of patients who died of severe acute asthma attack. **Chest 101**:916-921, 1992

18. Yamamoto A, Ishiguro H, Ko SB, et al: Ethanol induces fluid hypersecretion from guinea-pig pancreatic duct cells. **J Physiol 551**:917-926, 2003

19. Iplikcioglu AC, Bek S, Gokduman CA, et al: Diffuse villous hyperplasia of choroid plexus. **Acta Neurochir (Wien) 148**:691-694, 2006

20. D'Ambrosio AL, O'Toole JE, Connolly ES, Jr., et al: Villous hypertrophy versus choroid plexus papilloma: a case report demonstrating a diagnostic role for the proliferation index. **Pediatr Neurosurg 39**:91-96, 2003

21. Casey KF, Vries JK: Cerebral fluid overproduction in the absence of tumor or villous hypertrophy of the choroid plexus. **Childs Nerv Syst 5**:332-334, 1989

22. Gupta P, Sodhi KS, Mohindra S, et al: Choroid plexus papilloma of the third ventricle: A rare infantile brain tumor. **J Pediatr Neurosci 8**:247-249, 2013

23. Saito A, Nishimura S, Fujita T, et al: A case of difficult management of fluid-electrolyte imbalance in choroid plexus papilloma. **Neurol Med Chir (Tokyo) 54**:659-663, 2014

24. Rekate HL, Erwood S, Brodkey JA, et al: Etiology of ventriculomegaly in choroid plexus papilloma. **Pediatr Neurosci 12**:196-201, 1985

25. Kwon MS, Woo SK, Kurland DB, et al: Methemoglobin is an endogenous toll-like receptor 4 ligand-relevance to subarachnoid hemorrhage. **Int J Mol Sci 16**:5028-5046, 2015

26. Damkier HH, Brown PD, Praetorius J: Cerebrospinal fluid secretion by the choroid plexus. **Physiol Rev 93**:1847-1892, 2013

27. Keep RF, Xiang J, Betz AL: Potassium cotransport at the rat choroid plexus. **Am J Physiol 267**:C1616-C1622, 1994

28. Wu Q, Delpire E, Hebert SC, et al: Functional demonstration of Na+-K+-2Cl- cotransporter activity in isolated, polarized choroid plexus cells. **Am J Physiol 275**:C1565-C1572, 1998

29. Plotkin MD, Kaplan MR, Peterson LN, et al: Expression of the Na(+)-K(+)-2Cl- cotransporter BSC2 in the nervous system. **Am J Physiol 272**:C173-C183, 1997

30. Christensen HL, Nguyen AT, Pedersen FD, et al: Na(+) dependent acid-base transporters in the choroid plexus; insights from slc4 and slc9 gene deletion studies. **Front Physiol 4**:304, 2013

31. Praetorius J: Water and solute secretion by the choroid plexus. **Pflugers Arch 454**:1-18, 2007

32. Piechotta K, Lu J, Delpire E: Cation chloride cotransporters interact with the stress-related kinases Ste20-related proline-alanine-rich kinase (SPAK) and oxidative stress response 1 (OSR1). **J Biol Chem 277**:50812-50819, 2002

33. Begum G, Yuan H, Kahle KT, et al: Inhibition of WNK3 Kinase Signaling Reduces Brain Damage and Accelerates Neurological Recovery After Stroke. **Stroke 46**:1956-1965, 2015

34. Kahle KT, Ring AM, Lifton RP: Molecular physiology of the WNK kinases. **Annu Rev Physiol 70**:329-355, 2008

35. Gagnon KB, Delpire E: Molecular physiology of SPAK and OSR1: two Ste20-related protein kinases regulating ion transport. **Physiol Rev 92**:1577-1617, 2012

36. Gagnon KB, England R, Delpire E: Volume sensitivity of cation-Cl- cotransporters is modulated by the interaction of two kinases: Ste20-related proline-alanine-rich kinase and WNK4. **Am J Physiol Cell Physiol 290**:C134-C142, 2006

37. Yan Y, Dalmasso G, Nguyen HT, et al: Ste20-related proline/alanine-rich kinase (SPAK) regulated transcriptionally by hyperosmolarity is involved in intestinal barrier function. **PLoS One 4**:e5049, 2009

38. Park HW, Nam JH, Kim JY, et al: Dynamic regulation of CFTR bicarbonate permeability by [Cl-]i and its role in pancreatic bicarbonate secretion. **Gastroenterology 139**:620-631, 2010

39. Oreskovic D, Klarica M: The formation of cerebrospinal fluid: nearly a hundred years of interpretations and misinterpretations. **Brain Res Rev 64**:241-262, 2010

40. Karimy JK, Kahle KT, Kurland DB, et al: A novel method to study cerebrospinal fluid dynamics in rats. **J Neurosci Methods 241**:78-84, 2015

41. Krishnamurthy S, Li J, Schultz L, et al: Intraventricular infusion of hyperosmolar dextran induces hydrocephalus: a novel animal model of hydrocephalus. **Cerebrospinal Fluid Res 6**:16, 2009

42. Krishnamurthy S, Li J, Schultz L, et al: Increased CSF osmolarity reversibly induces hydrocephalus in the normal rat brain. **Fluids Barriers CNS 9**:13, 2012

43. Vogh BP, Godman DR, Maren TH: Effect of AlCl3 and other acids on cerebrospinal fluid production: a correction. **J Pharmacol Exp Ther 243**:35-39, 1987

44. Chiu C, Miller MC, Caralopoulos IN, et al: Temporal course of cerebrospinal fluid dynamics and amyloid accumulation in the aging rat brain from three to thirty months. **Fluids Barriers CNS 9**:3, 2012

45. Preston JE: Ageing choroid plexus-cerebrospinal fluid system. **Microsc Res Tech 52**:31-37, 2001

46. Romero-Calvo I, Ocon B, Martinez-Moya P, et al: Reversible Ponceau staining as a loading control alternative to actin in Western blots. **Anal Biochem 401**:318-320, 2010

47. Nugent BM, Valenzuela CV, Simons TJ, et al: Kinases SPAK and OSR1 are upregulated by estradiol and activate NKCC1 in the developing hypothalamus. **J Neurosci 32**:593-598, 2012

48. de Los HP, Alessi DR, Gourlay R, et al: The WNK-regulated SPAK/OSR1 kinases directly phosphorylate and inhibit the K+-Cl- co-transporters. **Biochem J 458**:559-573, 2014

49. Flatman PW: Regulation of Na-K-2Cl cotransport by phosphorylation and protein-protein interactions. **Biochim Biophys Acta 1566**:140-151, 2002

50. Kikuchi E, Mori T, Zeniya M, et al: Discovery of Novel SPAK Inhibitors That Block WNK Kinase Signaling to Cation Chloride Transporters. **J Am Soc Nephrol 26**:1525-1536, 2015

51. Lin GM, Liu PY, Wu CF, et al: Perspective of future drugs targeting sterile 20/SPS1-related proline/alanine-rich kinase for blood pressure control. **World J Cardiol 7**:306-310, 2015

52. Vitari AC, Deak M, Morrice NA, et al: The WNK1 and WNK4 protein kinases that are mutated in Gordon's hypertension syndrome phosphorylate and activate SPAK and OSR1 protein kinases. **Biochem J 391**:17-24, 2005

53. Clark RG, Milhorat TH, Stanley WC, et al: Experimental Pantopaque ventriculography. **J Neurosurg 34**:387-395, 1971

54. Thiery JC, Lomet D, Bougoin S, et al: Turnover rate of cerebrospinal fluid in female sheep: changes related to different light-dark cycles. **Cerebrospinal Fluid Res 6**:9, 2009

55. Pollay M, Stevens A, Estrada E, et al: Extracorporeal perfusion of choroid plexus. **J Appl Physiol 32**:612-617, 1972

56. Begley DJ: Delivery of therapeutic agents to the central nervous system: the problems and the possibilities. **Pharmacol Ther 104**:29-45, 2004

57. Blanchette M, Fortin D: Blood-brain barrier disruption in the treatment of brain tumors. **Methods Mol Biol 686**:447-463, 2011

58. Foust KD, Kaspar BK: Over the barrier and through the blood: to CNS delivery we go. **Cell Cycle 8**:4017-4018, 2009

59. Glascock JJ, Osman EY, Coady TH, et al: Delivery of therapeutic agents through intracerebroventricular (ICV) and intravenous (IV) injection in mice. **J Vis Exp** 2011

60. Pressler RM, Boylan GB, Marlow N, et al: Bumetanide for the treatment of seizures in newborn babies with hypoxic ischaemic encephalopathy (NEMO): an open-label, dose finding, and feasibility phase 1/2 trial. **Lancet Neurol 14**:469-477, 2015

61. Erker T, Brandt C, Tollner K, et al: The bumetanide prodrug BUM5, but not bumetanide, potentiates the antiseizure effect of phenobarbital in adult epileptic mice. **Epilepsia** 2016

62. Milhorat TH, Hammock MK, Davis DA, et al: Choroid plexus papilloma. I. Proof of cerebrospinal fluid overproduction. **Childs Brain 2**:273-289, 1976

63. Eisenberg HM, McComb JG, Lorenzo AV: Cerebrospinal fluid overproduction and hydrocephalus associated with choroid plexus papilloma. **J Neurosurg 40**:381-385, 1974

64. Trevisi G, Frassanito P, Di RC: Idiopathic cerebrospinal fluid overproduction: case-based review of the pathophysiological mechanism implied in the cerebrospinal fluid production. **Croat Med J 55**:377-387, 2014

65. Anei R, Hayashi Y, Hiroshima S, et al: Hydrocephalus due to diffuse villous hyperplasia of the choroid plexus. **Neurol Med Chir (Tokyo) 51**:437-441, 2011

66. Carrion E, Hertzog JH, Medlock MD, et al: Use of acetazolamide to decrease cerebrospinal fluid production in chronically ventilated patients with ventriculopleural shunts. **Arch Dis Child 84**:68-71, 2001

67. McCarthy KD, Reed DJ: The effect of acetazolamide and furosemide on cerebrospinal fluid production and choroid plexus carbonic anhydrase activity. **J Pharmacol Exp Ther 189**:194-201, 1974

68. Murphy VA, Johanson CE: Acidosis, acetazolamide, and amiloride: effects on 22Na transfer across the blood-brain and blood-CSF barriers. **J Neurochem 52**:1058-1063, 1989

69. Javaheri S, Wagner KR: Bumetanide decreases canine cerebrospinal fluid production. In vivo evidence for NaCl cotransport in the central nervous system. **J Clin Invest 92**:2257-2261, 1993

70. Knuckey NW, Fowler AG, Johanson CE, et al: Cisterna magna microdialysis of 22Na to evaluate ion transport and cerebrospinal fluid dynamics. **J Neurosurg 74**:965-971, 1991